INTERANNUAL ZONAL VARIABILITY OF THE COUPLED STRATOSPHERE-TROPOSPHERE CLIMATE SYSTEM

A Thesis
Presented to
The Academic Faculty

by

Benton W. Whitesides

In Partial Fulfillment
of the Requirements for the Degree
Master of Science in the
School of Earth and Atmospheric Sciences

Georgia Institute of Technology
August 2006

INTERANNUAL ZONAL VARIABILITY OF THE COUPLED STRATOSPHERE-TROPOSPHERE CLIMATE SYSTEM

Approved by:

Dr. Robert X. Black, Advisor
School of Earth and Atmospheric Sciences
Georgia Institute of Technology

Dr. Derek Cunnold
School of Earth and Atmospheric Sciences
Georgia Institute of Technology

Dr. Emanuele Di Lorenzo
School of Earth and Atmospheric Sciences
Georgia Institute of Technology

Date Approved: July 10, 2006

To my family of friends;
for sharing laughter and endless support.

ACKNOWLEDGEMENTS

I would like to thank my advisor, Dr. Robert X. Black, for offering his experience and guidance to this project and introducing me to many unanswered questions in climate variability. I especially want to thank my peers Dr. Brent McDaniel and Dr. Dennis Robinson for their contribution to computations in this project and for our equally important spirited office discussions. I would like to also acknowledge GT Research Scientist Muhammad Shaikh for helping perform CAM model simulations, Thomas Christian for modeling ideas, and the School of Earth and Atmospheric Sciences for providing me with the opportunity and challenge to be a better scientist.

TABLE OF CONTENTS

	Page
ACKNOWLEDGEMENTS	iv
LIST OF FIGURES	vii
LIST OF TABLES	x
LIST OF SYMBOLS AND ABBREVIATIONS	xi
SUMMARY	xii
CHAPTER 1: LITERATURE REVIEW	1
1.1 Introduction	1
1.2 Climatological Framework	1
1.3 Large-Scale Atmospheric Interannual Variability	7
CHAPTER 2: CALCULATIONS	15
2.1 Data	15
2.2 Methodology	16
CHAPTER 3: DYNAMIC STRUCTURES	22
3.1 El Nino Southern Oscillation	22
3.2 Quasi-Biennial Oscillation	28
3.3 Solar Variability	34
3.4 Volcanic Activity	41
CHAPTER 4: DIAGNOSTIC TOOLS	48
4.1 Eliassen-Palm Fluxes and Wave Driving	48
4.2 Stream Function Analyses	54
4.3 Potential Vorticity Inversions	56
4.4 Model Simulation of Solar Activity	63

CHAPTER 5: DISCUSSION 69

REFERENCES 73

LIST OF FIGURES

Page

Figure 1.1: Annual climatology (1958-2001) of zonal-average temperature (K). Warmest temperatures occur in equatorial regions at the surface while cool temperatures occur in the stratosphere above the same region and at the poles. Plots based on data from the NCEP/NCAR reanalyses project. 2

Figure 1.2: Zonally averaged zonal winds (m/s) for seasons (a) June through August (b) and December through February. In both hemispheres, regardless of season, there are strong mid-latitude westerly jets centered at the 300hPa pressure level. At higher altitudes strong stratospheric jets oscillate between winter westerly and summer easterly winds. Plots based on data from the NCEP/NCAR reanalyses project (1958-2001). 3

Figure 1.3: Schematic of meridional circulation induced to maintain thermal wind balance in response to wave breaking. Deceleration of the zonal mean wind necessitates meridional circulation to weaker temperature gradient. This involves both adiabatic warming poleward of and below the wave-breaking zone as well as adiabatic cooling equatorward of and below the wave-breaking zone. 5

Figure 1.4: Reprinted from Hurrell (2003). Variability in sea level pressure between high and low NAO index years. Solid lines indicate positive values, dashed lines indicate negative values, and intervals of the contours are 2 hPa. 8

Figure 1.5: Reprinted from Baldwin et al. (2001). Composite of zonal wind (m/s) oscillations associated with the QBO transitioning from easterlies to westerlies at 20hPa. Shading intervals of 5m/s. Units of the time delay are months. 10

Figure 1.6: 10.7cm solar flux, with a clearly dominant 11-year periodicity, is used as a proxy for the sunspot cycle. Based on National Geophysical Data Center measurements 12

Figure 1.7: Schematic of the impacts of stratospheric aerosol loading resulting from volcanic activity on atmospheric interannual variability. 14

Figure 2.1: Climatology of EP Fluxes (vectors) and Wave Driving (contours, m/s) during the NH cool season (Nov-Mar) compiled from NCEP data (1958-2001). EP Fluxes indicate wave propagation from the troposphere through the tropopause (indicated by a magenta contour) and into the stratosphere, subsequently slowing the zonal mean wind (negative anomalies). 21

Figure 3.1: Difference in zonal mean wind (m/s) between maximum and minimum ENSO during boreal cool seasons (1979-2001) in NCEP reanalyses at 6 months prior through 6 months after index extremes. Red (blue) shading indicates positive (negative) anomalies. Magenta contour indicates tropopause and green contours outline regions of significance of 95% or higher determined by a Student's T-test. 23

Figure 3.2: Same as Figure 3.1 except using ERA 40 data. 24

Figure 3.3: Same as Figure 3.1 except for Temperature (K). 25

Figure 3.4: Same as Figure 3.2 except for Temperature (K). 26

Figure 3.5: Variability between maximum and minimum ENSO index extremes in Temperature (left, K) and Zonal Wind (right, m/s) during boreal cool seasons for the extended time period (1958-2001) in NCEP (top) and ERA 40 (bottom) reanalyses. Red (blue) shading indicates positive (negative) anomalies. Magenta contour indicates tropopause and green contours outline regions of significance of 95% or higher determined by a Student's T-test. 27

Figure 3.6: Same as Figure 3.1 except for the QBO. 29

Figure 3.7: Same as Figure 3.6 except using ERA 40 data. 30

Figure 3.8: Same as Figure 3.6 except for Temperature (K). 31

Figure 3.9: Same as Figure 3.7 except for Temperature (K). 32

Figure 3.10: Same as Figure 3.5 except for the QBO. 33

Figure 3.11: Same as Figure 3.3 except for solar variability. 36

Figure 3.12: Same as Figure 3.11 except using ERA 40 data. 37

Figure 3.13: Same as Figure 3.11 except for Zonal Winds (m/s). 38

Figure 3.14: Same as Figure 3.12 except for Zonal Winds (m/s). 39

Figure 3.15: Same as Figure 3.5 except for solar variability. 40

Figure 3.16: Same as Figure 3.3 except for volcanic activity. Lag 0 through 6. 43

Figure 3.17: Same as Figure 3.16 except using ERA 40 data. 44

Figure 3.18: Same as Figure 3.16 except for Zonal Winds (m/s). 45

Figure 3.19: Same as Figure 3.17 except for Zonal Winds (m/s). 46

Figure 3.20: Same as Figure 3.5 except for volcanic activity. 47

Figure 4.1: Variability between maximum and minimum ENSO in Eliassen-Palm Fluxes (Vectors) and Wave Driving (Contours, m/s/day) during boreal cool seasons (1979-2001) in ERA 40 reanalyses at 6 months prior through 6 months after index extremes. Red (blue) shading indicates positive (negative) anomalies. Magenta contour indicates tropopause. 50

Figure 4.2: Same as Figure 4.1 except for the QBO. 51

Figure 4.3: Same as Figure 4.1 except for solar variability. 52

Figure 4.4: Same as Figure 4.1 except for volcanic activity. Lag 0 through 6. 53

Figure 4.5: Anomalous stream function associated with modulation of ENSO, QBO, solar variability and volcanic activity during boreal cool seasons (1979-2001) in ERA ECMWF reanalysis. 55

Figure 4.6: Variability in zonal mean wind (m/s) associated with ENSO. Left: As seen in Figures 3.1 and 3.2 at lag 0, but isolated to the Northern Hemisphere. Center: Variability derived from the total PV anomaly field. Right: Variability derived from stratospheric PV anomalies. Upper panels use NCEP/NCAR ralanlyses. Lower panels use ERA reanalyses. 59

Figure 4.7: Same as Figure 4.6 except for the QBO. 60

Figure 4.8: Same as Figure 4.6 except for solar variability. 61

Figure 4.9: Same as Figure 4.6 except for volcanic activity. 62

Figure 4.10: Differences in 50mb Temperature between cases 1 through 5 and the control case. Warmer (cooler) shades indicate positive (negative) temperature anomalies. Contours and shading are held constant. 66

Figure 4.11: Same as Figure 4.10 except for Zonal Wind. 67

Figure 4.12: Same as Figure 4.10 except for EP Fluxes and Wave Driving. Magenta contour indicates approximate level of the tropopause. 68

LIST OF TABLES

Page

Table 4.1: Table of parameters increased in each case run. 63

LIST OF SYMBOLS AND ABBREVIATIONS

BD Circulation	Brewer-Dobson Circulation
CAM	Community Atmosphere Model
ECMWF	European Centre for Medium-Range Weather Forecasts
ENSO	El Nino Southern Oscillation
EP Flux	Eliassen-Palm Flux
GCM	General Circulation Model
NCAR	National Center for Atmospheric Research
NCEP	National Centers for Environmental Protection
NH	Northern Hemisphere
PNJ	Polar Night Jet
PV	Potential Vorticity
QBO	Quasi-Biennial Oscillation
SH	Southern Hemisphere
SSW	Sudden Stratospheric Warming Event
TEM	Transformed-Eulerian Mean
TSI	Total Solar Irradiance

SUMMARY

Understanding the dynamical relationships between low frequency forcings and the interannual variability of the Earth's atmosphere is critical for accurate extended-range forecasts and climate prediction. This thesis investigates possible dynamical couplings between the stratosphere and troposphere by implementing lagged multivariate linear regressions. These regressions were chosen to untangle the separate responses of distinct atmospheric forcings upon zonal mean climate variability. The regressions incorporate monthly meteorological data with indices of four dominant forcings of low frequency atmospheric variability: the El Nino Southern Oscillation, the Quasi-Biennial Oscillation, the 11-year solar cycle, and volcanic activity. The analysis uses data from both the NCAR/NCEP and ECMWF reanalyses for two distinct time periods to expose possible satellite measurement influences. One period consists of all data since 1958, while the other period includes only data since 1979, a period of extensive satellite observations. Diagnostic tools include piecewise potential vorticity inversions, an assessment of anomalous Eliassen-Palm fluxes, stream function analyses, and general circulation model diagnoses. The examination reveals robust patterns associated with each forcing, consistent with existing theories in climate dynamics of the coupling mechanisms between the stratosphere and the troposphere. To better predict climate variability, however, the next step is to investigate the nonlinearities known to play an important role in this system.

CHAPTER 1

LITERATURE REVIEW

Preceding the calculation details and results performed in this study, a literature review will first be presented expressing current scientific theories and the importance of this study on the subjects of stratosphere-troposphere coupling and interannual climate variability.

1.1 Introduction

The relationship between solar variability and atmospheric dynamics has long been suspected, but previous data limitations and lack of mechanistic explanations have lead to an increased focus on interannual climate variability (Baldwin and Dunkerton 2004). Isolation of the solar signal has been difficult because of the slow variations in the sunspot cycle which are often overshadowed by interference with other atmospheric forcings. It is known, however, that stratospheric ozone is highly sensitive to incoming ultraviolet radiation. Heating due to this ozone significantly impacts stratospheric climate. It is critical to understand the dynamical link between solar variability and the earth's atmosphere for successful extended range weather forecasting and climate prediction (Baldwin and Dunkerton 2004). The goal of this study is to isolate signals of the El Nino-Southern Oscillation, the Quasi-Biennial Oscillation, and volcanic activity from that of the 11-year solar cycle. A complication to this task is the known interaction of each phenomenon with one another.

1.2 Climatological Framework

The mean state of the atmosphere, common patterns of variability, and major forcings on the climate system must first be examined in order to gain an understanding

of the mechanisms of interannual climate variability. Atmospheric temperature and wind fields within the troposphere and stratosphere and their seasonal variability will be the first to be discussed. For the entirety of this thesis, zonal-mean structures (i.e. how they appear once averaged around a latitudinal circle) will be considered.

1.2.1 Temperature and Wind Structures

The annual average climatological zonal-mean temperature field, presented in Figure 1.1, illustrates high equatorial surface temperatures in the troposphere which decrease with increasing altitude and latitude. Temperatures rise due to high ozone concentrations above the level of the tropopause, shown as the heavy black contour [using the WMO thermal tropopause definition (Lewis 1991)]. In the stratosphere, the mean horizontal temperature gradient is opposite of the troposphere, but there is substantial seasonal variability. Much cooler temperatures occur over the winter poles, most apparent during Southern Hemisphere (SH) winter (Grotjahn 2003).

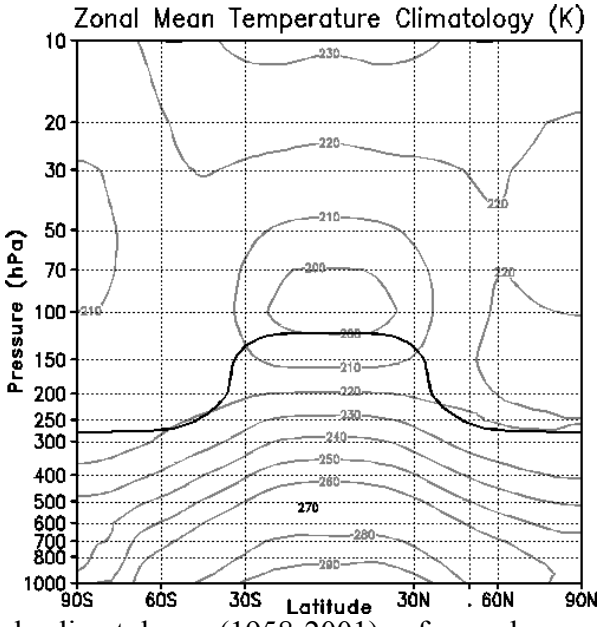

Figure 1.1. Annual climatology (1958-2001) of zonal-average temperature (K). Warmest temperatures occur in equatorial regions at the surface while cool temperatures occur in the stratosphere above the same region and at the poles. Plots based on data from the NCEP/NCAR reanalyses project.

Thermal wind balance directly links seasonal variability in the temperature field to variability in the zonal-mean wind fields. Thermal wind balance relates the latitudinal temperature gradient to the vertical shear of the zonal wind: as the temperature gradient between the tropics and the poles increases, so does the vertical wind shear (Holton 1992). Figure 1.2 contrasts the climatological zonal-mean zonal wind field between winter and summer. The troposphere of both summer and winter hemispheres is dominated by easterly winds in the tropics and strong westerly jets in the mid-latitudes. Within the stratosphere however, winds vary greatly between winter and summer hemispheres (Grotjahn 2003). A strong westerly flow, known as the stratospheric polar vortex, can be seen at high latitudes in the winter stratosphere, especially during the SH winter. This polar vortex isolates cold polar air masses from warmer air masses at lower latitudes (Wallace 2003). Conversely, in the summer hemisphere, the stratospheric polar vortex vanishes and the stratosphere is dominated by an easterly flow.

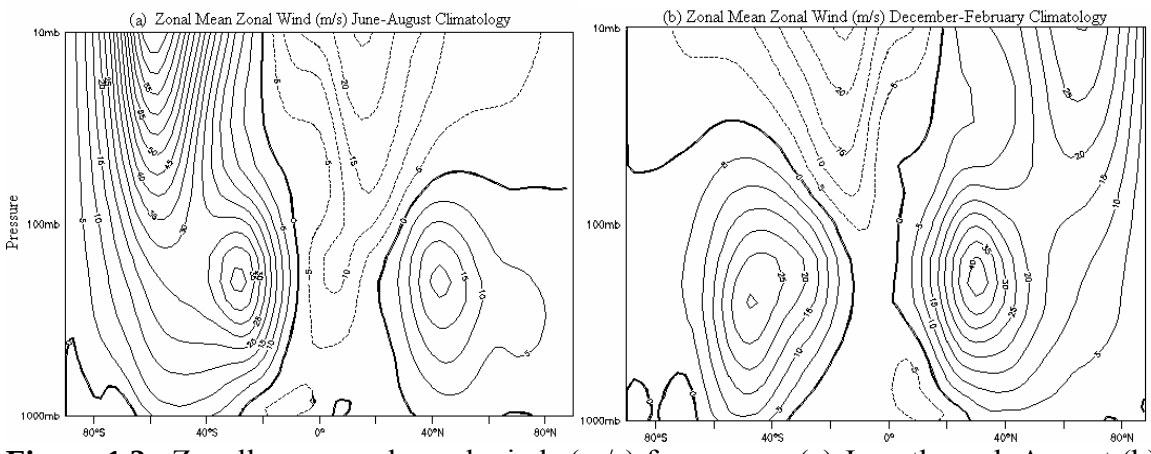

Figure 1.2. Zonally averaged zonal winds (m/s) for seasons (a) June through August (b) and December through February. In both hemispheres, regardless of season, there are strong mid-latitude westerly jets centered at the 300hPa pressure level. At higher altitudes strong stratospheric jets oscillate between winter westerly and summer easterly winds. Plots based on data from the NCEP/NCAR reanalyses project (1958-2001).

The transition period between winter and summer is critical in the understanding of the dynamic coupling of the troposphere and stratosphere and the impact of solar variability. In early winter, the mean stratospheric zonal circulation is radiatively driven by spatial variations in solar heating. As winter progresses, the circulation pattern becomes increasingly more dynamically driven by vertically propagating tropospheric planetary (Rossby) waves. The stratospheric polar vortex moves to higher latitudes and begins to weaken with this transition (Kodera and Kuroda 2002).

1.2.2 Stratosphere-Troposphere Coupling

There are several mechanisms through which the stratosphere and troposphere are linked to one another. It is commonly accepted that one way the stratosphere influences the troposphere is by regulating how much ultraviolet radiation passes through. It is also well understood that the troposphere influences the stratosphere through the upward propagation of planetary waves from the troposphere, which greatly impact atmospheric temperature, wind, and ozone fields among others (Smith 2003). This investigation focuses on less well-understood dynamics that couple the stratosphere-troposphere system once these waves propagate into the stratosphere and then provide feedback to the troposphere.

A planetary Rossby wave is a latitudinal displacement of a fluid that retains its potential vorticity (PV). The wave's restoring motion drives the wave and makes potential vorticity displacement reversible. These waves are vertically evanescent in summer easterlies, but are able to propagate vertically into the stratosphere in wintertime westerlies (Wallace and Hobbs 1977). In early winter, waves are ducted towards the equator, but in late winter, waves are ducted poleward, causing poles to warm, and the polar vortex to weaken (Boville 1986). This response occurs because of nonlinear wave breaking (irreversible PV displacement) in areas of strong vertical wind shear. At this critical level of wave breaking, linear assumptions break down, wave amplitude increases

and velocity of wave propagation drops to zero. When this wave breaking occurs, temperature fluxes carried directly by the planetary waves have little impact in an Eulerian mean sense, but the Transformed Eulerian Mean (TEM) represents how the zonal mean flow locally responds to the eddy forcing (Wallace and Hobbs 1977, Andrews, Holton and Levoy 1987).

At the critical level of wave breaking there is an equatorward transport of potential vorticity, therefore maximum deceleration of the zonal mean wind occurs at this level. Wave breaking deposits negative wave drag at this critical level weakening the polar vortex. This weakening is known as *wave driving*. To main thermal wind balance, the underlying temperature gradient is reduced via an induced meridional circulation which adiabatically warms (cools) the atmosphere poleward (equatorward) of the wave-breaking zone as illustrated in Figure 1.3. This meridional circulation involves rising motion in the atmosphere equatorward of the breaking event, poleward motion across the critical level, sinking motion in the atmosphere poleward of the breaking event, and a return flow below the critical level.

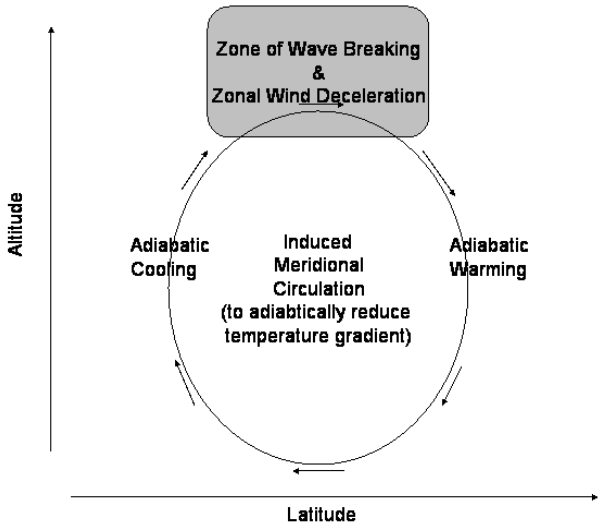

Figure 1.3 Schematic of meridional circulation induced to maintain thermal wind balance in response to wave breaking. Deceleration of the zonal mean wind necessitates meridional circulation to weaker temperature gradient. This involves both adiabatic

warming poleward of and below the wave-breaking zone as well as adiabatic cooling equatorward of and below the wave-breaking zone.

Even a small vertical air parcel displacement can result in significant temperature anomalies because of the strong temperature stratification within the stratosphere (Wallace and Hobbs 1977). Strong events of this nature are often referred to as sudden stratospheric warmings (SSW). When the polar vortex is strong, it allows less wave activity to propagate in, allowing it to remain in its radiative state for an extended period before migrating northward during the dynamically driven stage when SSW events are common (Kodera and Kuroda 2005).

Initially, a stratospheric dynamic influence on the troposphere was only thought to be capable through dramatic planetary wave redirection (Andrews, Holton and Levoy 1987). However, once the stratosphere has been influenced by tropospheric planetary waves, it then has the ability to feed back to the troposphere through a mechanism termed *downward control*. Once the vortex has been decelerated by wave breaking, and poleward motions are induced at the critical layer to maintain thermal wind balance, the subsequent meridional circulation reaches a steady state after adjustments in radiative cooling and friction occur within the troposphere. This adjustment is known as the *downward control* of the stratosphere on the troposphere (Haynes 2005).

The downward control mechanism is a focus of current research of stratosphere-troposphere coupling. Song and Robinson (2004) argue that the direct downward control influence on the troposphere is weak and must be reinforced by tropospheric eddies, wave number four and higher. However, Thompson, Furtado, and Shepherd (now in press) present modeling results to indicate that even after including tropospheric frictional drag, the downward control mechanism is of sufficient magnitude to account for observed tropospheric variability once the meridional circulation is enhanced by excess radiative cooling at high latitudes.

The stratospheric meridional circulation associated with downward control also causes a meridional transport of mass in the atmosphere from tropics to high latitudes, known as the Brewer-Dobson Circulation. This circulation is driven by wave-mean flow interactions in the Transformed Eulerian Mean explained in the previous section (Andrews, Holton and Levoy 1987). Through this mechanism, angular momentum (not heat) is transferred by planetary waves from the surface, driving poleward motion at the level of wave breaking, upwelling with adiabatic cooling in tropics, and downwelling with adiabatic warming at high latitudes (Shepherd 2002).

The downward propagation of zonal wind anomalies due to fluctuating Rossby waves in the troposphere is neither an effect of planetary wave reflection nor of the meridional circulation associated with downward control. Stratospheric zonal wind anomalies propagate downward in a similar way to SSW events (Plumb 2003). The inability of waves to propagate through easterly winds causes the waves to break at levels below this critical level. This leads to the downward propagation of the critical layer. Critical layers actually sink in the lower latitudes first, trapping waves at higher latitudes which then finally decelerate the polar vortex to the critic level. Once this occurs, the downward propagation can occur at latitudes of the polar vortex (Matsuno 1971).

1.3 Large-Scale Atmospheric Interannual Variability

With knowledge of the coupled stratosphere-troposphere climate system, we may begin to understand some aspects of its interannual variability. This year to year variability can be characterized as the difference between a monthly average for a particular year, and a monthly average over many years. The primary mode of interannual variability in the extratropical troposphere is the North Atlantic Oscillation (NAO). This surface pattern is strikingly similar to the Arctic Oscillation (AO) but without a pacific center of action, which when extended into higher levels of the atmosphere is known as the Northern Annular Mode (NAM) (Thompson and Wallace

1998, Baldwin and Dunkerton 2004). Four of the most dominant forcings of interannual variability in the zonal-mean are the El Nino Southern Oscillation, the Quasi-Biennial Oscillation, the 11-year solar cycle, and volcanic activity. Each of these forcings is discussed in detail throughout the rest of this chapter.

1.3.1 The North Atlantic Oscillation

The North Atlantic Oscillation (NAO) is a pattern centered over the Atlantic Ocean in the Northern Hemisphere (NH) which has a large impact on the regional climate. The NAO is most often defined as a regional North-South oscillation in sea level pressure (Hurrell 2003). In winter, this pattern is coupled with the Stratosphere. This pattern is demonstrated in sea level pressure differences between high and low NAO index winters created by Hurrell (2003) shown in Figure 1.4.

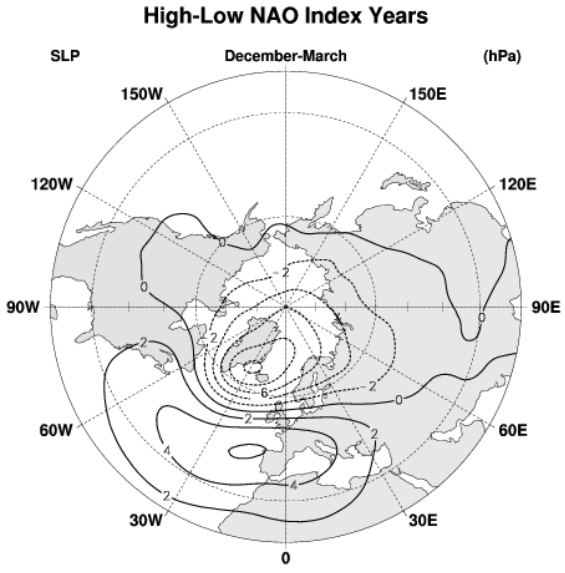

Figure 1.4 Reprinted from Hurrell (2003). Variability in sea level pressure between high and low NAO index years. Solid lines indicate positive values, dashed lines indicate negative values, and intervals of the contours are 2 mb.

For the positive phase of the NAO, sea level pressure anomalies are as in the pattern in Figure 1.4. Negative sea level pressure anomalies over the North Atlantic and positive

sea level pressure anomalies farther south drive strong westerly wind anomalies across the North Atlantic and Western Europe. In the opposite phase, the anomalous circulation pattern is reversed (Hurrell 2003).

1.3.2 El Nino Southern Oscillation

The dominant forcing of atmospheric interannual variability is the El Nino-Southern Oscillation (ENSO), a pattern that cycles every 2 to 7 years over the tropical Pacific. The cycle is a coupled oscillation between anomalous sea surface temperatures (SSTs) and variations in the Walker Circulation, a zonal circulation pattern driven by the surface temperature gradient. In the Walker Circulation, atmospheric convection occurs in regions of high surface temperature, and subsidence occurs in cooler regions (Chang and Zebiak 2003).

The El Nino phase of the oscillation is characterized by anomalously warm SSTs in the eastern equatorial Pacific. The weaker meridional temperature gradient leads to a weakening of easterly surface winds, suppressing normal upwelling of cold waters along the eastern edge of the basin, therefore providing a feedback mechanism for El Nino to grow and persist (Nichols 2003). The positive phase of ENSO is also associated with constructive interference of the extratropical climatological stationary waves and the Pacific North American (PNA) teleconnection pattern (a ridge over the Pacific Northwest with troughs to the east and west). This leads to increased wave propagation into the stratosphere and a relatively weak NH stratospheric polar vortex. During this phase, there are an increased number of SSW events. Both positive ENSO and SSW events have similar responses in the NH and, if the occur at the same time, the total warming response in the polar region may be greatly amplified (Taguchi and Hartman, 2005).

The La Nina phase occurs oppositely when sea surface temperatures are anomalously high in the western region of the basin and cold to the east, increasing the gradient in SSTs and therefore increasing easterly surface winds. Increased surface

winds draw more surface water away from the eastern edge of the basin, allowing more cold water upwelling to occur, helping the La Nina Phase to grow and persist (Nichols 2003). This phase has reduced vertical wave propagation and a stronger stratospheric polar vortex in the NH extratropics.

1.3.3. The Quasi-Biennial Oscillation

The Quasi-Biennial Oscillation (QBO) is a long-term oscillation pattern in the tropical stratospheric zonal wind, characterized by an alternation between easterly and westerly winds over the equator with a period of just over two years. This pattern is driven by the momentum forcing from several types of vertically propagating waves: particularly gravity, Rossby, and Kelvin waves (Baldwin et al. 2001). The downward propagation of zonal wind anomalies from the stratosphere to the troposphere is illustrated in the zonal wind composites of Figure 1.5. Substantial temperature anomalies (±4K) within the stratosphere result from the variability in vertical wind shear.

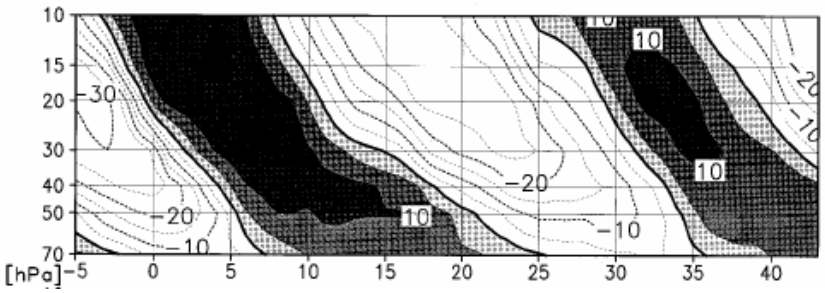

Figure 1.5 Reprinted from Baldwin et al. (2001). Composite of zonal wind (m/s) oscillations associated with the QBO transitioning from easterly to westerly at 20hPa. Shading intervals of 5m/s. Units of the time delay are months.

Impacts of the QBO can extend into the extra-tropics and include a modulation of the strength of the stratospheric polar vortex via the so-called *Holton-Tan Effect*. The Holton-tan effect is a result of alterations in the local structure and location of the stratospheric Rossby wave guide and critical line. The westerly phase of the QBO is associated with increased high latitude westerlies in the NH due to a southward redirection of propagating waves emanating from the troposphere (Baldwin et al. 2001).

The Holton-Tan effect is characterized by a strengthened polar vortex during a westerly QBO and stronger wave number one activity in early easterly QBO winters (Andrews, Holton and Levoy 1987). The Holton-Tan Mechanism is best depicted by removing extreme ENSO years from consideration as ENSO and QBO Signals may be similar in the extratropics (Baldwin et al. 2001).

Nonlinear effects of the QBO include interactions with annual cycle, temperature, ozone concentration, and vertical wind shear. This closely links the QBO to anomalous conditions forced by ENSO, solar variability and volcanic activity (Cordero and Nathan 2004, Baldwin et al. 2001). For example, increased solar flux is linked with a shortened duration of the westerly phase of the QBO and weakened westerly flow in extra-tropical winter regions during the easterly phase of the QBO (McCormack 2004). In addition, the Holton-Tan effect is apparent during low solar activity but the inverse response occurs during solar maximum (Baldwin et al., 2001). Also during solar maximum, there are more SSW events: 64% propagate down during solar maximum, whereas none propagate down during solar minimum (Hameed, 2005).

1.3.4. Solar Variability

Production of stratospheric ozone is highly sensitive to variability in ultraviolet radiation associated with the 11-year solar cycle. Ozone concentrations have a substantial impact on global temperature distribution and the subsequent atmospheric circulation. Observations of solar irradiance began in the 1950s, when technology was inadequate for precise measurements, but by the 1980s measurements had greatly improved (Rottman 1999). Total solar radiation varies only a tenth of a percent over the 11-year cycle, but ultraviolet (UV) radiation varies by several percent (at times over a factor of two at short UV wavelengths) (Baldwin and Dunkerton 2004). This 11-year periodicity can be observed in Figure 1.6: the 10.7cm solar flux, a proxy for sunspot numbers obtained from the National Geophysical Data Center. The 10.7cm solar flux is

the radiation emitted from the sun in the vicinity of sunspots at a wavelength of 10.7cm observed by the solar radio telescope. The variability in solar irradiance is linked to changes in the sun's magnetic field (Haigh 2003). In regions of strong magnetic fields, sunspots, cool dark regions on the sun's surface, are surrounded by stronger bright regions called faculae. The combined effect of sunspots and faculae is a net increase in solar irradiance. Therefore, when the number of sunspots is high, solar irradiance is also high. Sunspot variability is driven by a reversal in active regions of the sun's magnetic field that occurs on a 22-year cycle (Wallace and Hobbs 1977).

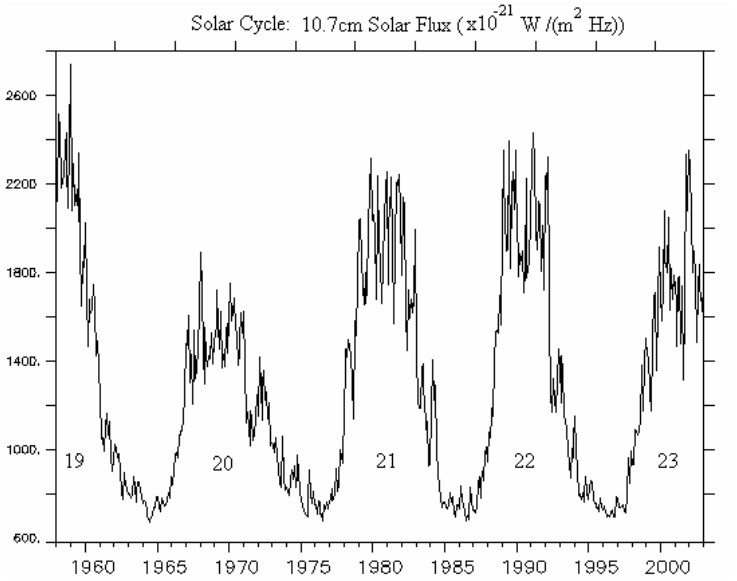

Figure 1.6. 10.7cm solar flux, with a clearly dominant 11-year periodicity, is used as a proxy for the sunspot cycle. Based on National Geophysical Data Center measurements.

The earth's atmosphere absorbs the majority of solar UV radiation with wavelengths of 300nm or smaller. Absorption of this short wave radiation occurring in the middle atmosphere aids the production of ozone, which causes localized heating and blocks the short wave radiation from reaching lower levels (Haigh 2003). Therefore, small changes in irradiance can lead to significant changes in other atmospheric processes (Rottman 1999). Modeling evidence has shown that small changes in UV radiation and ozone in the stratosphere project significantly on the troposphere (Reid 1998). Heating of the stratosphere associated with UV absorption may impact the troposphere through

associated dynamics including vertically propagating Rossby waves in winter (Haigh 2003). This response to solar variability occurs in each hemisphere's winter and involves the downward, poleward propagation of temperature and zonal wind anomalies by Rossby waves (Rozanov 2004, Baldwin and Dunkerton 2004). At solar maximum, the strongest, most significant warming occurs in the subtropical lower stratosphere and midlatitude troposphere (Haigh 2002) driving meridional circulation anomalies in order to maintain thermal wind balance. This results in an intensification of the polar vortex, and decreased temperatures at high latitudes in the lower stratosphere (Rozanov 2004).

Within the troposphere, warming is observed at all latitudes with maximum in solar activity (Coughlin 2004). The mechanisms thought to explain these anomalies involves diabatic heating of stratospheric ozone, subsequent increase of infrared radiation into the troposphere, and dynamical mechanisms introduced by Kodera and Kuroda (2002). Kodera and Kuroda (2005) explain that during winters of solar maximum, enhanced stratospheric ozone heating at low latitudes strengthens the polar vortex, allowing it to remain for an extended period in a radiatively driven state, and delays its northward progression. Circulation anomalies resulting from this are consistent with the pattern of the NAO in the NH. Like the NAO, the Southern Annular Mode (SAM) in the SH displays similar wintertime variability linked to solar activity. Kodera and Kuroda (2003) also demonstrate that the Brewer Dobson circulation is weakened during solar maximum because planetary waves are redirected toward the equator and tropical upwelling is decreased. This further increases temperature in the equatorial stratosphere, decreases ozone transport towards each pole, and reinforces anomalously cool polar temperatures (Kuroda and Kodera 2005).

1.3.5. Volcanic Activity

Large volcanic eruptions influence climate by sending aerosols and gasses into the stratosphere where they may reside for several years. However, some eruptions,

which do not force aerosols into the stratosphere, produce only local effects (Robock 2003). Though stratospheric aerosol clouds decrease ozone levels throughout the stratosphere by acting as a medium for ozone reducing chemistry, there is also increased warming of the stratosphere though absorption of short- and long-wave radiation. Despite the net warming in the stratosphere, stratospheric aerosol clouds block solar radiation into the troposphere leading to anomalous cooling at the surface for several years after the eruption (with the exception of warmer winter temperatures over land in the NH) (Robock 2003). Aerosol heating in the tropical stratosphere leads to an enhanced temperature gradient and polar vortex within the winter stratosphere associated with a positive AO response. This system is schematically represented in Figure 1.7. The response may be muted or amplified when it occurs simultaneously with other events (e.g. decreased effect of El Chichon eruption during an El Nino). Long term climate feedbacks include a carbon cycle feedback and water vapor feedback ending in decreased carbon dioxide, water vapor and global temperature (Robock 2003).

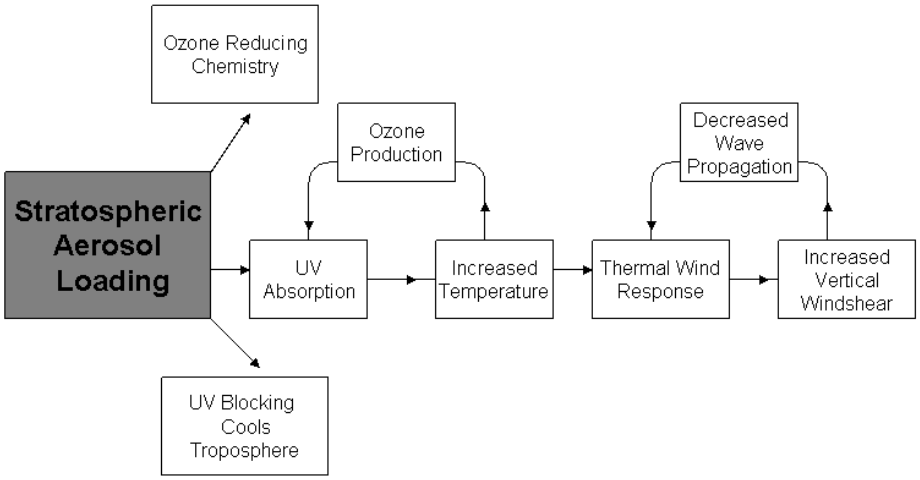

Figure 1.7. Schematic of the impacts of stratospheric aerosol loading resulting from volcanic activity on atmospheric interannual variability.

CHAPTER 2

CALCULATIONS

In order to isolate anomalies in the stratosphere and troposphere associated with each phenomenon, calculations in this study were performed using lagged multivariate linear regressions with monthly reanalysis data. This chapter provides detailed discussion of the data used, methodology, and other specific diagnostic tools used in these analyses.

2.1 Data

2.1.1. Anomaly Fields

In this investigation, two reanalyses datasets were examined in order to determine possible dataset biases: the National Centers for Environmental Prediction / National Center for Atmospheric Research (NCEP/NCAR) reanalyses and the ERA40 dataset. The NCEP/NCAR reanalyses dataset (Kalnay et al. 1996) was provided by the NOAA-CIRES ESRL/PSD Climate Diagnostics branch, Boulder, Co, and is available from their website at http://www.cdc.noaa.gov/. The ERA40 reanalyses dataset was compiled by the European Centre for Medium-Range Weather Forecasts (ECMWF), and is also available online at http://www.ecmwf.int/. Both data sets are arranged on a spatial grid with a horizontal resolution of 2.5˚ latitude by 2.5˚ longitude. For this analysis, 17 pressure levels (from 1000hPa to 10hPa) are used, but it should be noted that the ECMWF reanalyses provides additional pressure levels above 10hPa.

2.1.2. Independent Regression Indices

In the multivariate linear regression, indices for all previously described low frequency forcings were incorporated using monthly and spatially invariant time series.

As a representation of the El Nino-Southern Oscillation, a monthly Cold Tongue Index (a measurement of eastern equatorial Pacific sea surface temperature anomalies), was obtained from the Joint Institute for the Study of the Atmosphere and Ocean at the University of Washington, and is accessible online: http://tao.atmos.washington.edu/data_sets/cti/.

This regression also employs zonal winds at 30hPa over Singapore to represent the phase of the Quasi-Biennial Oscillation. This data may be obtained from the Climate Prediction Center: http://www.cpc.ncep.noaa.gov/data/indices/qbo.u30.index.

As a proxy for the 11-year Sunspot Cycle, the 10.7cm solar flux estimates were obtained from the National Geophysical Data Center. This data is available at the following ftp site: ftp://ftp.ngdc.noaa.gov/STP/SOLAR_DATA/SOLAR_RADIO/FLUX/MONTHLY.OBS.

To account for volcanic activity in the analysis, monthly stratospheric aerosol optical depths (550nm) are included from the NASA Goddard Institute for Space Studies (online at www.giss.nasa.gov/data/strataer/tau_line.txt). For the period between 1960 and 1978 (before implementation of extensive satellite measuring capabilities) this optical depth measurement was based primarily on observations of solar eclipse brightness. After 1978, optical depth has been measured by the Stratospheric Aerosol Monitor and Stratospheric Aerosol and Gas Experiment from a satellite view of solar occultation, supplemented at times by balloon, aircraft and ground-based measurements (Sato 1993).

2.2 Methodology

The goal of this investigation is to identify the atmospheric response within the coupled stratosphere-troposphere system to changes in low frequency forcing to better improve regional climate forecasts. Results of this regression provide a platform for

discussion of the dynamic couplings between the stratosphere and troposphere discussed in further detail in later chapters.

2.2.1. Anomaly Fields

Monthly anomaly fields were compiled from our two reanalysis data sources for temperature, winds, and geopotential height fields. Daily averages provided by NCEP/NCAR and the ECMWF (as well as daily calculated eddy heat and momentum fluxes) were first converted into anomalies from daily climatology by the explicitremoval of annual and semiannual components of a Fourier analysis of daily data. The anomalies were then averaged into monthly means and zonally averaged. From this, the residual long term average was removed, followed by the removal of the long-term linear trend. The long term average and linear trends vary for different time spans as described in the following section.

2.2.2. Seasonal Stratification and Time Spans

Once anomaly fields are created, they are binned into different time periods to determine the impact of satellite technology on the data. One dataset is compiled using all data from the 23 year period for which satellites have been fully implemented (1979-2001), henceforth referred to as *post-satellite*. Additionally, a longer dataset was also created using all anomaly data for the entire 43 year time span (1958-2001), henceforth referred to as the *extended* time span. Long term means and trends are calculated individually for each time span. It is important to note that differences between the two time periods may be attributable to factors other than the implementation of comprehensive satellite measuring capabilities.

Because of the strong seasonal variability of the atmospheric circulation, we will also seasonally stratify the data in order to perform isolated analysis of NH winters, when planetary waves have the ability to propagate into the stratosphere (Baldwin and

Dunkerton 2004). Bins used for seasonal stratification include a NH Cool Season (November-March) and a NH Warm Season (May-September). This stratification reveals the influence of seasonal dynamics on the zonal-mean response.

2.2.3. Regressions

The analysis is performed using multivariate linear regressions to be described in the following sections in detail. Though these regressions are useful tools for separating superimposed signals, there are two cautionary points that must be kept in mind when interpreting the results: 1) Nonlinearities between the independent variables of the regression are not accounted for and 2) the short temporal length of reliable data during low-frequency events does not always facilitate a clear or significant signal. To address this problem, we must additionally develop longer reliable data sets in the future, and compare current observational results to General Circulation Models.

2.2.3.1 Multivariate Linear Regressions

The multivariate linear regression used in this investigation incorporates monthly anomaly fields with the aforementioned atmospheric low-frequency forcings: the El Nino Southern Oscillation, the Quasi-Biennial Oscillation, solar variability, and volcanic activity. Three similar regression studies are referenced for comparison. Labitzke (2003) uses a simple linear regression between observations and the 10.7cm solar flux, while two other works (Gleisner and Thejll 2003; Haigh 2003) incorporate a multivariate linear regression to also include the El Nino Southern Oscillation and optical thickness, as a proxy for volcanic activity. Haigh (2003) additionally incorporates the Quasi-Biennial Oscillation in the same manner.

The equation for the multivariate linear regression procedure can be expressed at each grid point as the following function:

$$Y_t = \beta_E X_{E,t=lag} + \beta_S X_{S,t=lag} + \beta_V X_{V,t=lag} + \beta_Q X_{Q,t=lag} + \beta_{Auto} Y_{t-1} + \varepsilon_t \quad (1)$$

Where Y represents any observed monthly mean anomaly field: i.e. zonal wind, temperature, geopotential height, as well as eddy heat and momentum fluxes. X_{ind} represents each phenomenological index: the Cold Tongue Index (ENSO), the 10.7cm solar flux, stratospheric aerosol thickness (Volcanic Activity), 30hPa Singapore winds at month t (QBO), and the regressed variable one month before to account for autocorrelation. β_{Ind} represents the unknown regression coefficient and ε_t is the error for each month t. This can be written more simply in matrix form as [Y] = [X][β] + [ε], which expands at each grid point to:

$$\begin{bmatrix} \\ Y_1 \\ Y_2 \\ \vdots \\ Y_t \end{bmatrix} = \begin{bmatrix} X_{Enso,2} & X_{Solar,2} & \cdots & Y_1 \\ X_{Enso,3} & X_{Solar,3} & \cdots & Y_2 \\ \vdots & \vdots & & \vdots \\ X_{Enso,t} & X_{Solar,t} & \cdots & Y_{t-1} \end{bmatrix} \begin{bmatrix} \beta_{Enso} \\ \beta_{Solar} \\ \beta_{Volc} \\ \beta_{Qbo} \\ \beta_{Auto} \end{bmatrix} + \begin{bmatrix} \\ \varepsilon_2 \\ \varepsilon_3 \\ \vdots \\ \varepsilon_t \end{bmatrix} \qquad (2)$$

Using the method of least squares, the equation for the unknown regression coefficient matrix can be written as $[\beta] = ([X]'[X])^{-1}[X]'[Y]$ (Bethea 1995). By solving for the unknown regression coefficient at each grid point, we are able to identify the signature of solar variability on monthly anomalies independent of the other phenomena incorporated in the regression.

2.2.3.2 Temporal Lag Regressions

Multivariate regressions are expanded temporally through time lags ranging from negative to positive six months. This expansion is incorporated into the analysis for the purpose of understanding the temporal evolution of such anomalies as individual forcings strengthen and weaken.

2.2.4. Potential Vorticity Inversions

The downward and poleward expansion of stratospheric zonal wind anomalies has been linked to momentum transport from planetary Rossby waves driven along a gradient in potential vorticity (PV) (Baldwin and Dunkerton 2004). Rossby waves are largely forced by topography and land-sea contrasts, therefore, greater activity occurs in the NH, which has more surface area covered by land then the SH.

Quasi-geostrophic PV is defined by the following equation using the anomalous geopotential, Φ:

$$PV \equiv \frac{\nabla^2 \Phi}{f} + f + \left(\frac{f}{\sigma} \frac{\partial \Phi}{\partial p} \right) \qquad (3)$$

Where σ is the static stability parameter (Holton 1992). This conservative property relates relative and planetary vorticity to stretching vorticity, which is a function of temperature stratification. This equation demonstrates that anomalous potential vorticity in a given location is directly related to geopotential anomalies. In a quasi-geostrophic system, motions are in hydrostatic and geostrophic balance; therefore, local PV anomalies are associated with non-local geostrophic wind anomalies. Once potential vorticity anomalies are calculated and potential vorticity inversions are performed to determine induced geostrophic winds, ageostrophic components may also be estimated by comparison with raw wind anomalies of each forcing. Also, source regions of induced geostrophic wind anomalies may be identified by comparing anomalies induced by potential vorticity anomalies in selected areas, in this case, the stratosphere and troposphere.

2.2.5. Eliassen-Palm Fluxes and Wave Driving

The impact of Rossby waves can be diagnosed using the transformed Eulerian mean, where the effects of eddies can be directly assessed. In this context, wave

propagation in the meridional plane is given by the Eliassen–Palm (EP) flux vector, F, where components F_y and F_z are defined in Cartesian coordinates:

$$F_y = -\rho_o \overline{u'v'}; F_z = f_o \rho_o R \frac{\overline{v'T'}}{N^2 H} \quad (4)$$

In these equations, ρ_o is reference density, N^2 is the Buoyancy frequency, H is the scale height, prime denotes deviation from the zonal mean, and overbar represents the zonal average (Holton 1992). Monthly values for eddy heat and momentum fluxes applied to this calculation were obtained by making monthly and zonal averages of daily fluxes. Variability in anomalous EP flux was used to calculate the associated acceleration or deceleration of mean zonal wind due to large scale eddies (Baldwin, 1985). Figure 2.1 illustrates the climatology of this interaction during the NH cool season.

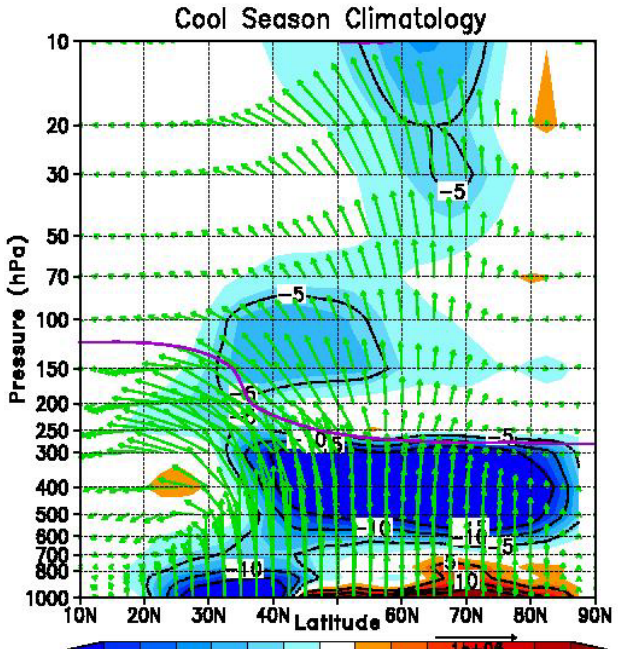

Figure 2.1 Climatology of EP Fluxes (vectors) and Wave Driving (contours, m/s) during the NH cool season (Nov-Mar) compiled from NCEP data (1958-2001). EP Fluxes indicate wave propagation from the troposphere through the tropopause (indicated by a magenta contour) and into the stratosphere, subsequently slowing the zonal mean wind (negative anomalies).

CHAPTER 3

DYNAMIC STRUCTURES

We will first examine regression results for basic temperature and zonal wind anomaly fields associated with each index. Anomalies are presented in terms of maximum variability in the forcing (i.e. the difference between a forcing index maximum and minimum). Emphasis is placed on the post-satellite time period in the NH which provides the most confidence, while results are also included for the SH and extended time periods. For the entirety of this study, contours and shading will be held constant within, but vary between, each index. Significance levels of 95% or higher using a student's t-test are indicated in all Figures in this chapter by green contours.

3.1 El Nino - Southern Oscillation

We first examine the difference in evolution between El Nino and La Nina. Within the NH, observations are consistent between datasets and significant at the 95% level or higher in regions outlined with a green contour. With the winter onset of the ENSO maximum, the stratospheric polar vortex is weakened and shifted south, remaining in this state for several months (See figures 3.1 and 3.2). This is matched by the replacement of the cool winter polar stratosphere with warm anomalies in both the NCEP and ERA datasets (Figures 3.3 and 3.4 respectively). These observations are consistent with other studies (e.g. Lorenz and Hartman 2003), as well as the theory introduced in Chapter 1 that, during El Nino, constructive interference of the PNA pattern with climatological stationary waves causes enhanced vertical propagation of planetary waves, slowing the polar night jet and raising stratospheric temperatures above the winter pole. When the regression is extended to include the extended time series (1958-2001), the same features are observed (Figure 3.5).

ENSO: Zonal Wind Evolution in NCEP data over Cool Seasons (1979-2001)

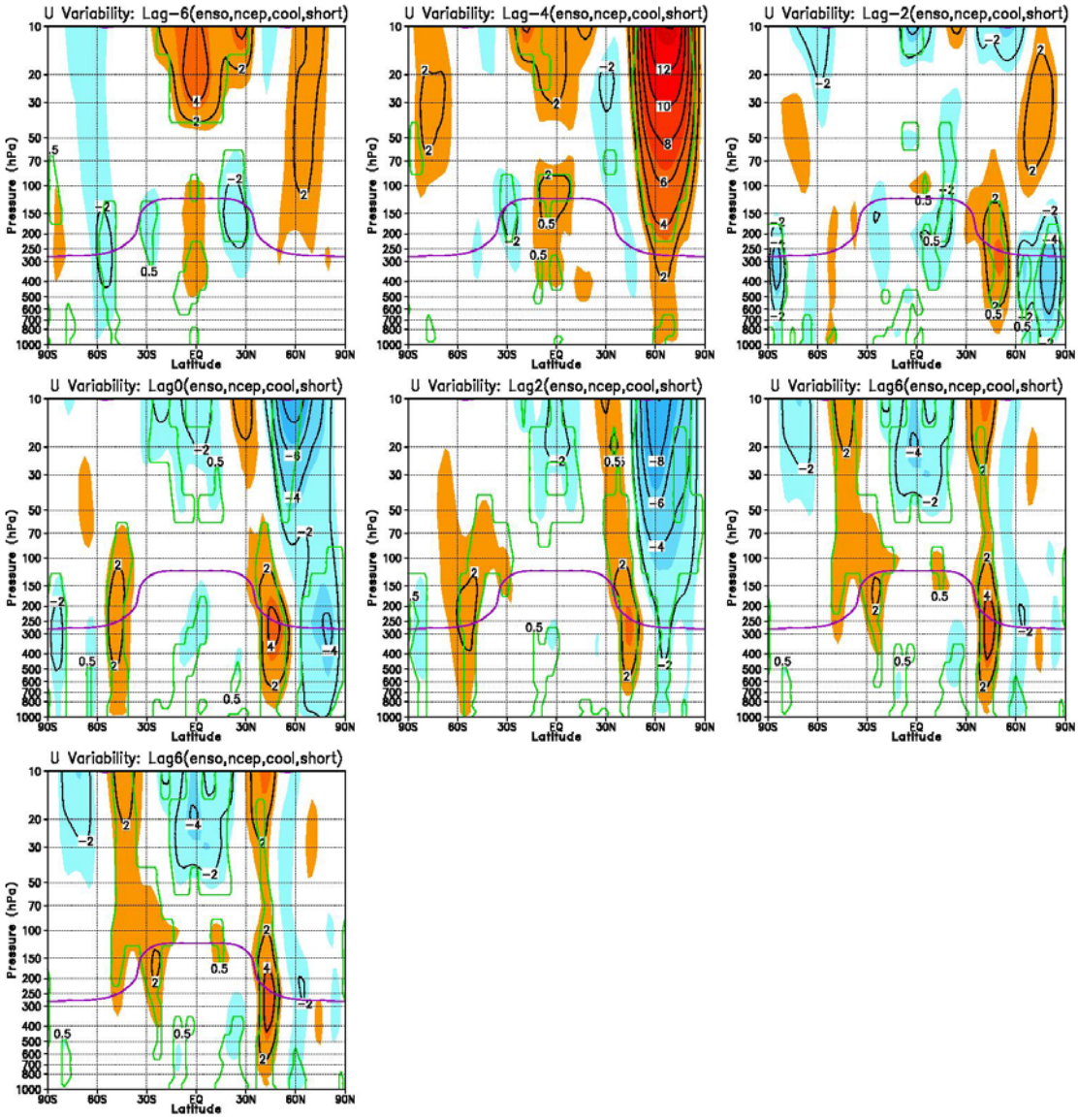

Figure 3.1. Zonal mean wind (m/s) difference between maximum and minimum ENSO during boreal cool seasons (1979-2001) in NCEP reanalyses at 6 months prior through 6 months after index extremes. Red (blue) shading indicates positive (negative) anomalies. Magenta contour indicates tropopause and green contours outline regions of significance of 95% or higher determined by a Student's T-test.

ENSO: Zonal Wind Evolution in ERA data over Cool Seasons (1979-2001)

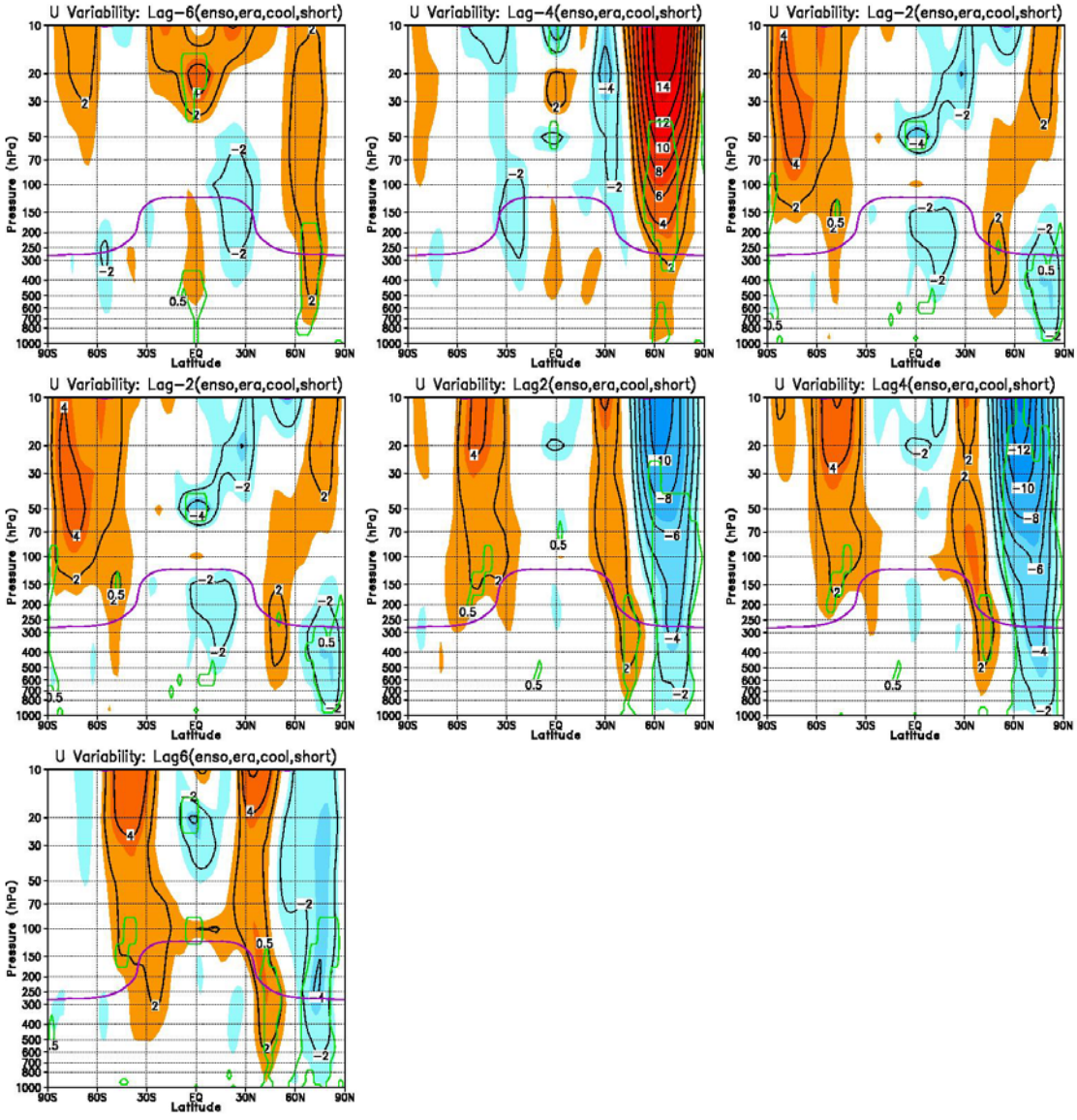

Figure 3.2. Same as Figure 3.1 except for ERA 40 data**.**

ENSO: Temperature Evolution in NCEP data over Cool Seasons (1979-2001)

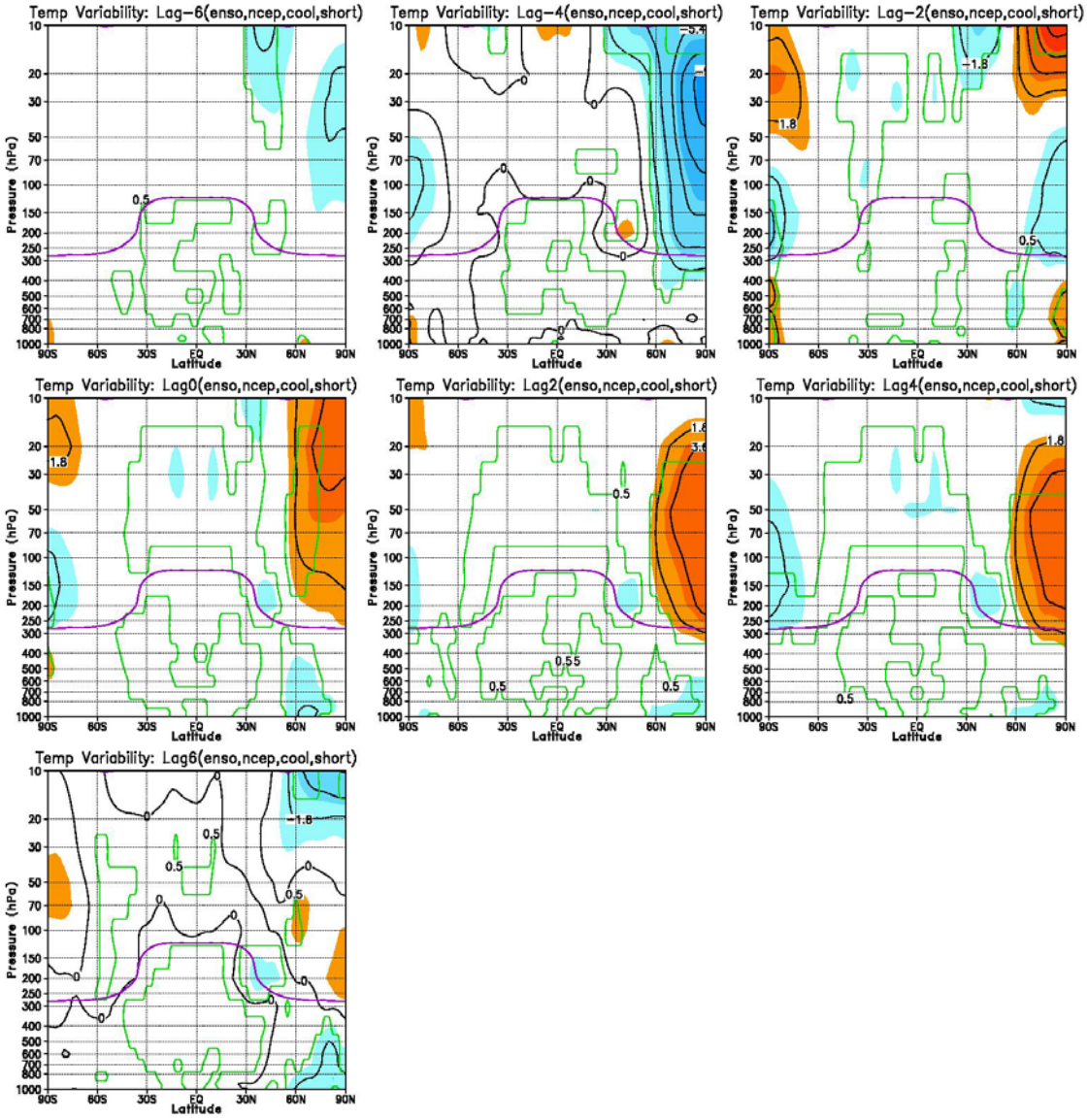

Figure 3.3. Same as Figure 3.1 except for Temperature (K).

ENSO: Temperature Evolution in ERA data over Cool Seasons (1979-2001)

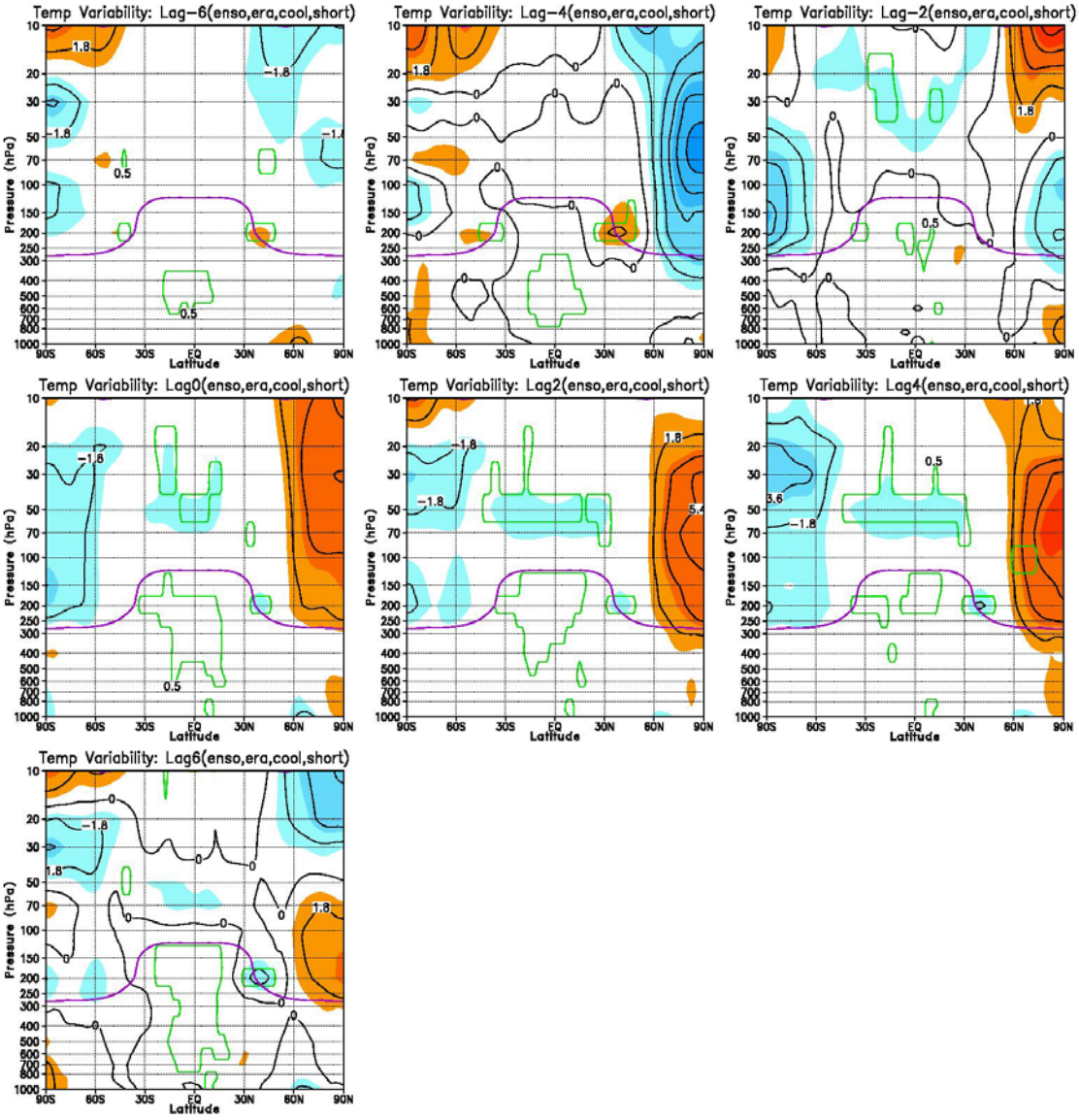

Figure 3.4. Same as Figure 3.2 except for Temperature (K).

ENSO: Zonal Wind in NCEP and ERA during Cool Seasons

Extended time Period **(1958-2001)**

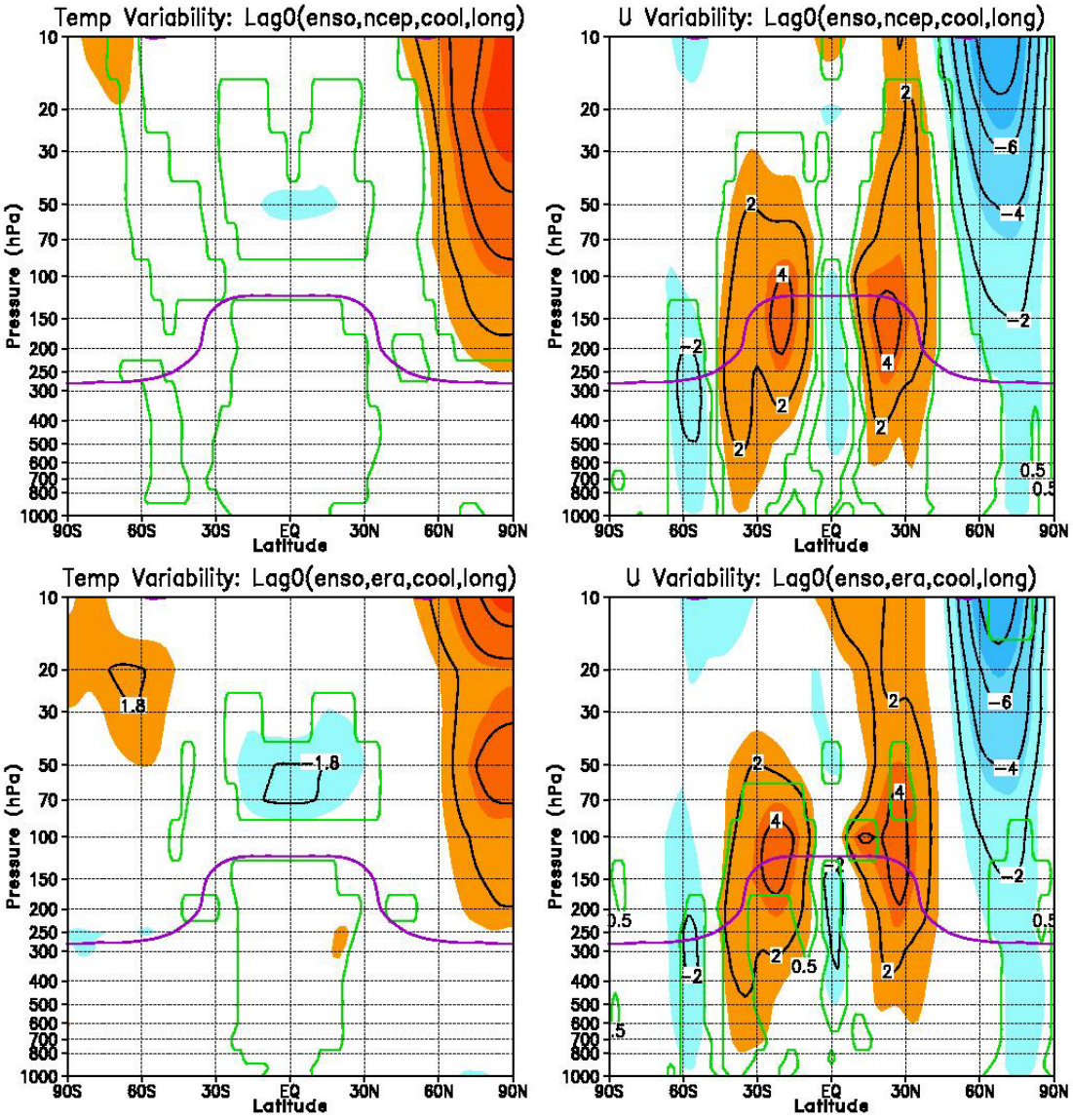

Figure 3.5. Variability in Temperature (left, K) and Zonal Wind (right, m/s) between maximum and minimum ENSO index extremes during boreal cool seasons for the extended time period (1958-2001) in NCEP (top) and ERA 40 (bottom) reanalyses. Red (blue) shading indicates positive (negative) anomalies. Magenta contour indicates tropopause and green contours outline regions of significance of 95% or higher determined by a Student's T-test**.**

3.2 The Quasi-Biennial Oscillation

The QBO results show the expected intensification of the stratospheric polar vortex during the westerly phase of the QBO, described in Chapter 1 as the Holton- Tan effect. Figures 3.6 and 3.7 illustrate the replacement of easterly anomalies by westerlies in the wintertime polar stratosphere. At the same time, westerly wind anomalies also descend at high latitudes of the SH (significant at a level of 95% or higher in the NCEP dataset). Observations of evolution in the temperature field during onset of the QBO (Figures 3.8 and 3.9) reveal a stratospheric cooling above the northern polar region. This is consistent with an increase in the stratospheric polar vortex. At the level where the QBO index is measured (30-50mb), observations reveal a significant warming. In the SH, both datasets show considerable cooling of the polar stratosphere. In the extended time period (Figure 3.10), stronger warming in the tropical lower stratosphere, cooling in the stratosphere at both the North and South poles, and enhancement of stratospheric westerlies at mid to high latitudes occur at levels of high significance in the Northern Hemisphere.

QBO: Zonal Wind Evolution in NCEP data over Cool Seasons (1979-2001)

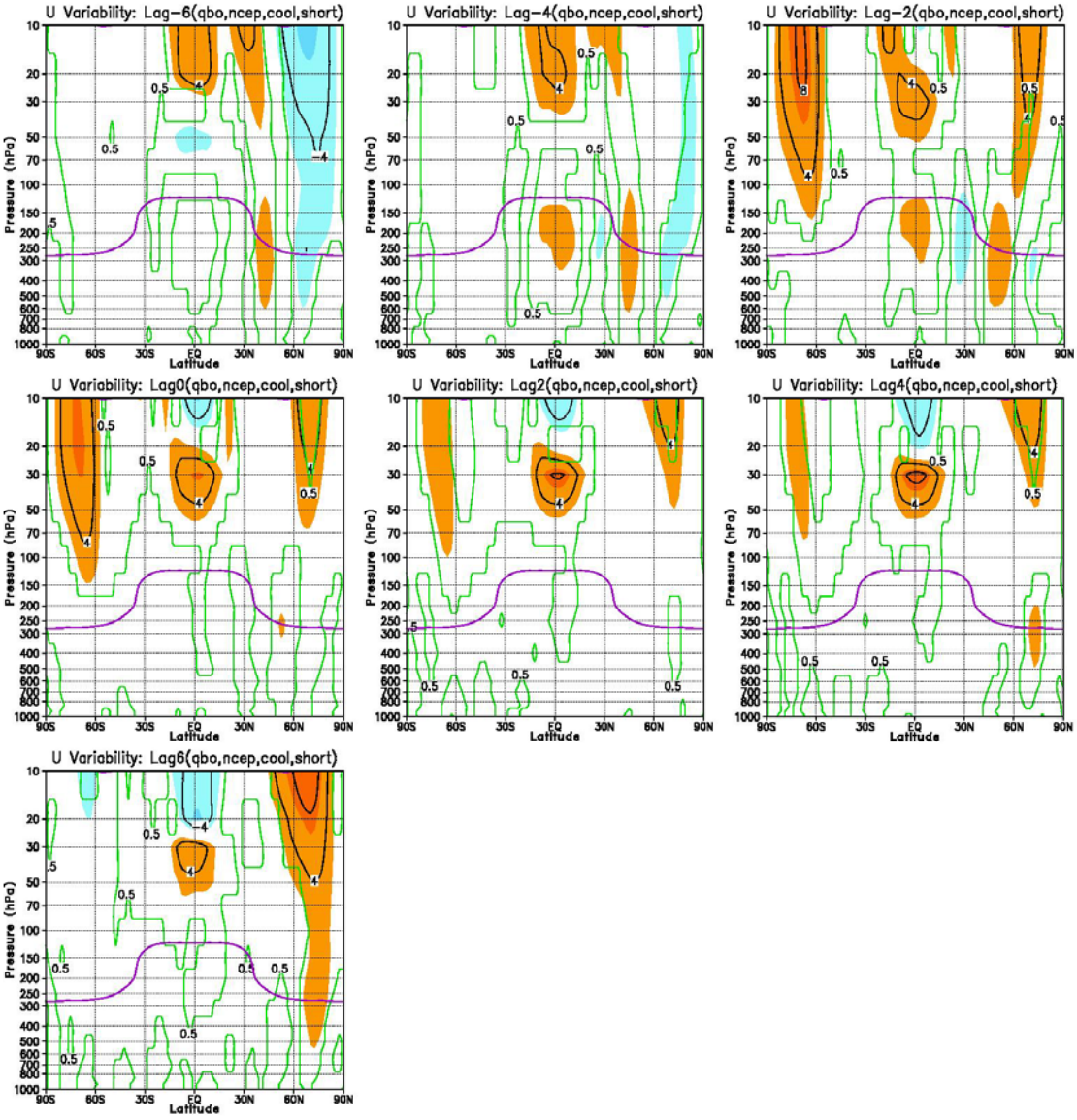

Figure 3.6. Variability in zonal mean wind (m/s) between maximum and minimum QBO during boreal cool seasons (1979-2001) in NCEP reanalyses at 6 months prior through 6 months after index extremes. Red (blue) shading indicates positive (negative) anomalies. Magenta contour indicates tropopause and green contours indicate regions of significance of 95% or higher determined by a Student's T-test.

QBO: Zonal Wind Evolution in ERA data over Cool Seasons (1979-2001)

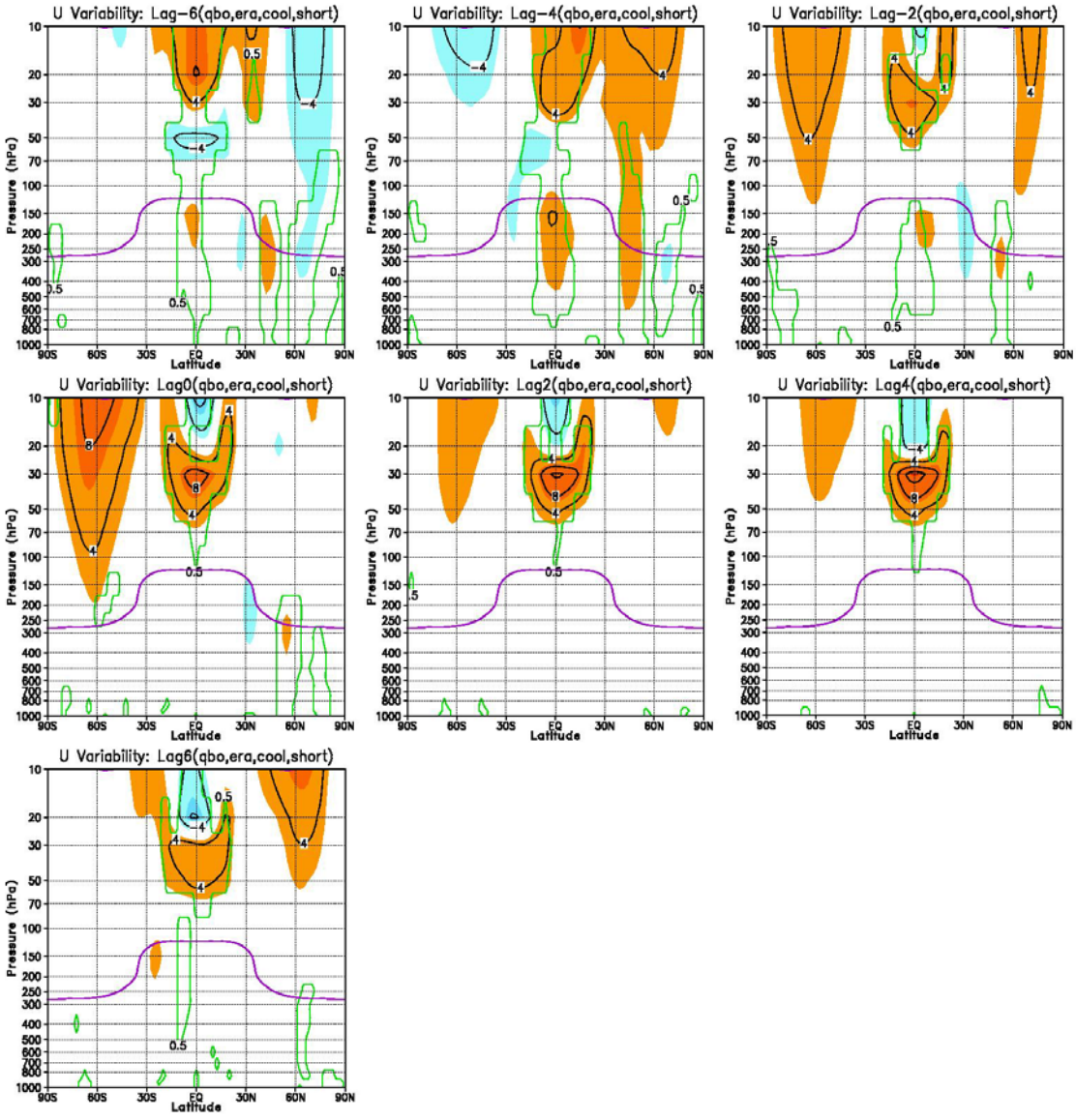

Figure 3.7. Same as Figure 3.6 except using ERA 40 data**.**

QBO: Temperature Evolution in NCEP data over Cool Seasons (1979-2001)

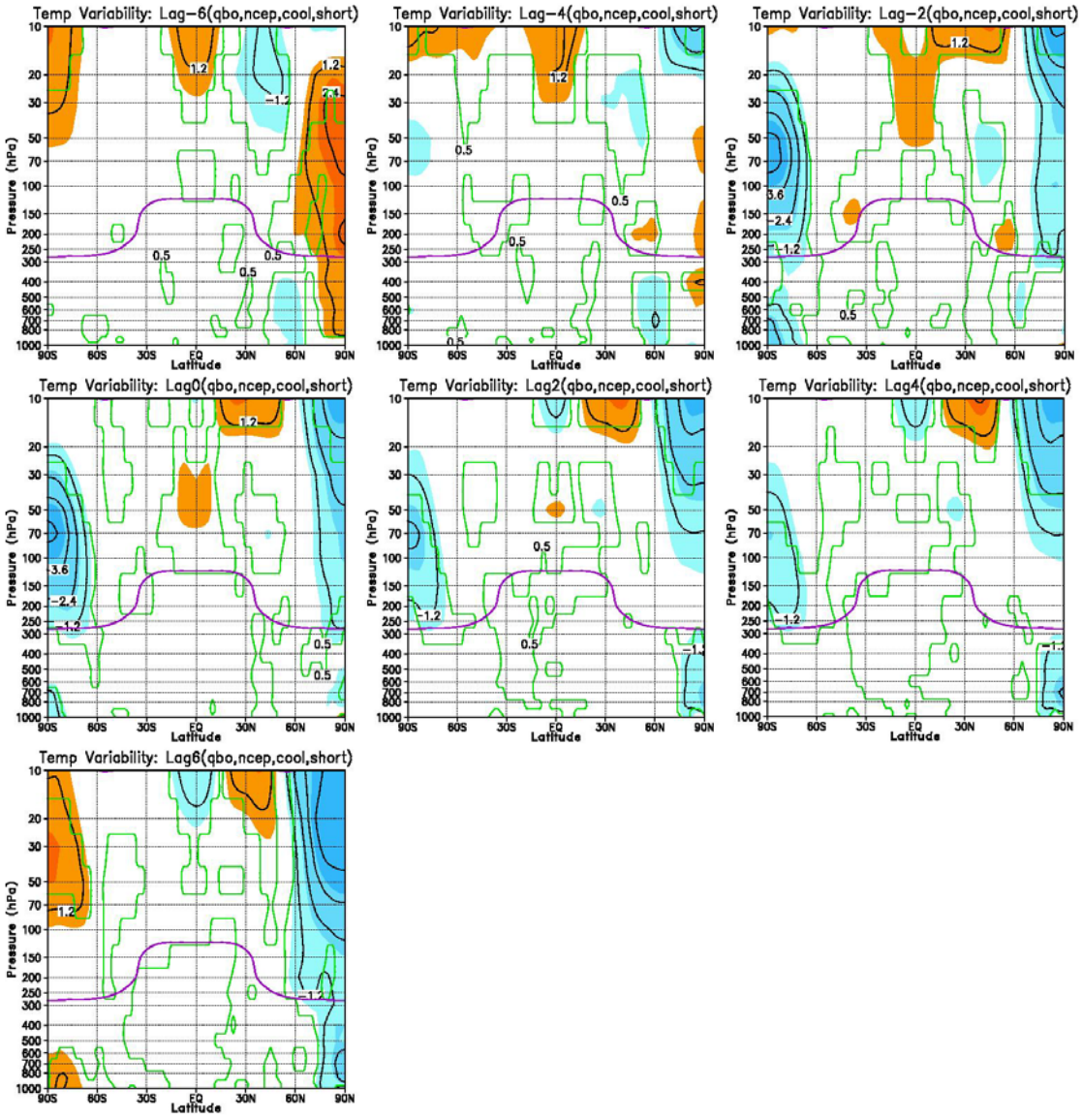

Figure 3.8. Same as Figure 3.6 except for Temperature (K)**.**

QBO: Temperature Evolution in ERA data over Cool Seasons (1979-2001)

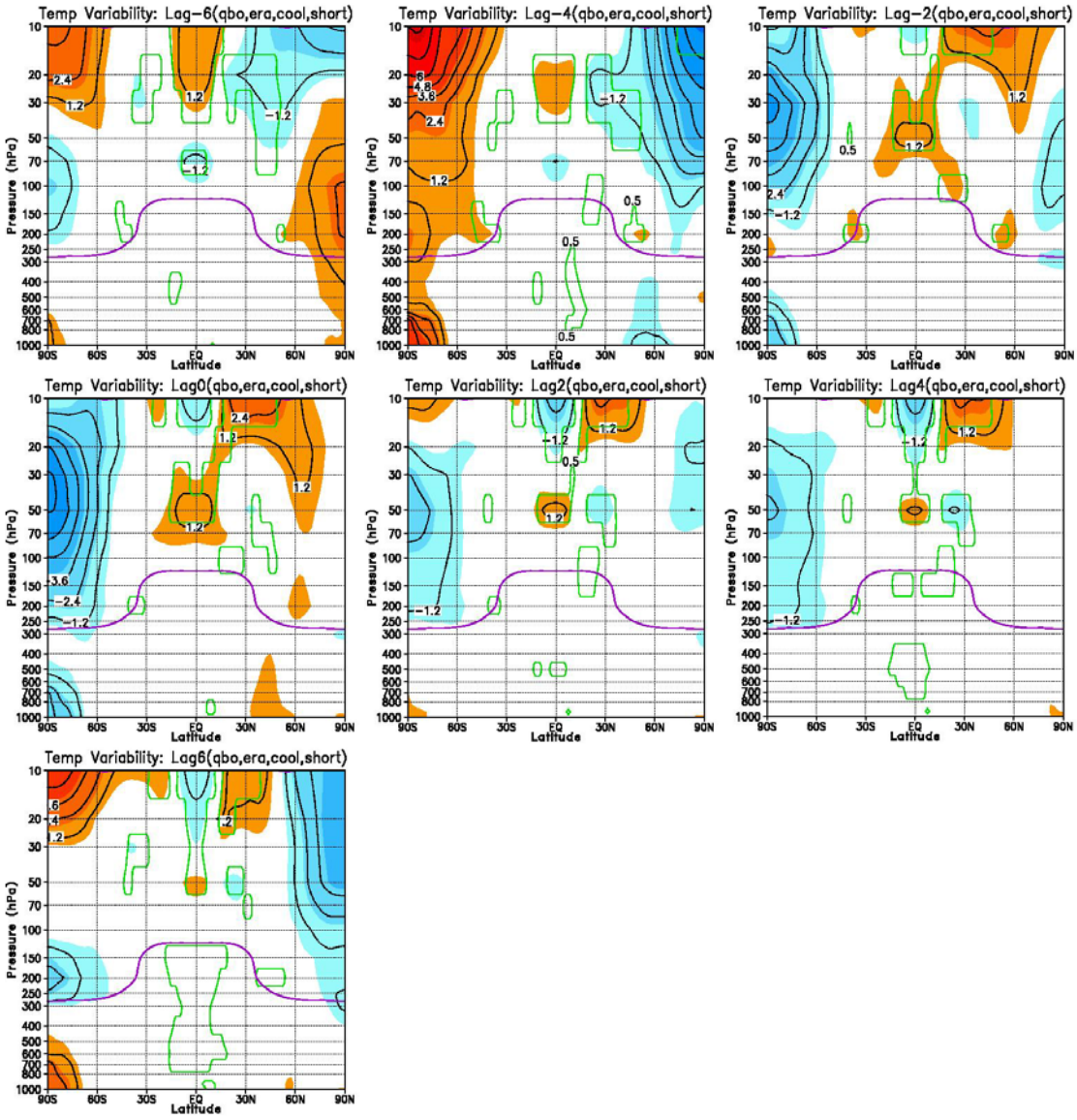

Figure 3.9. Same as Figure 3.7 except for Temperature (K).

QBO: Zonal Wind in NCEP and ERA during Cool Seasons

***Extended time Period* (1958-2001)**

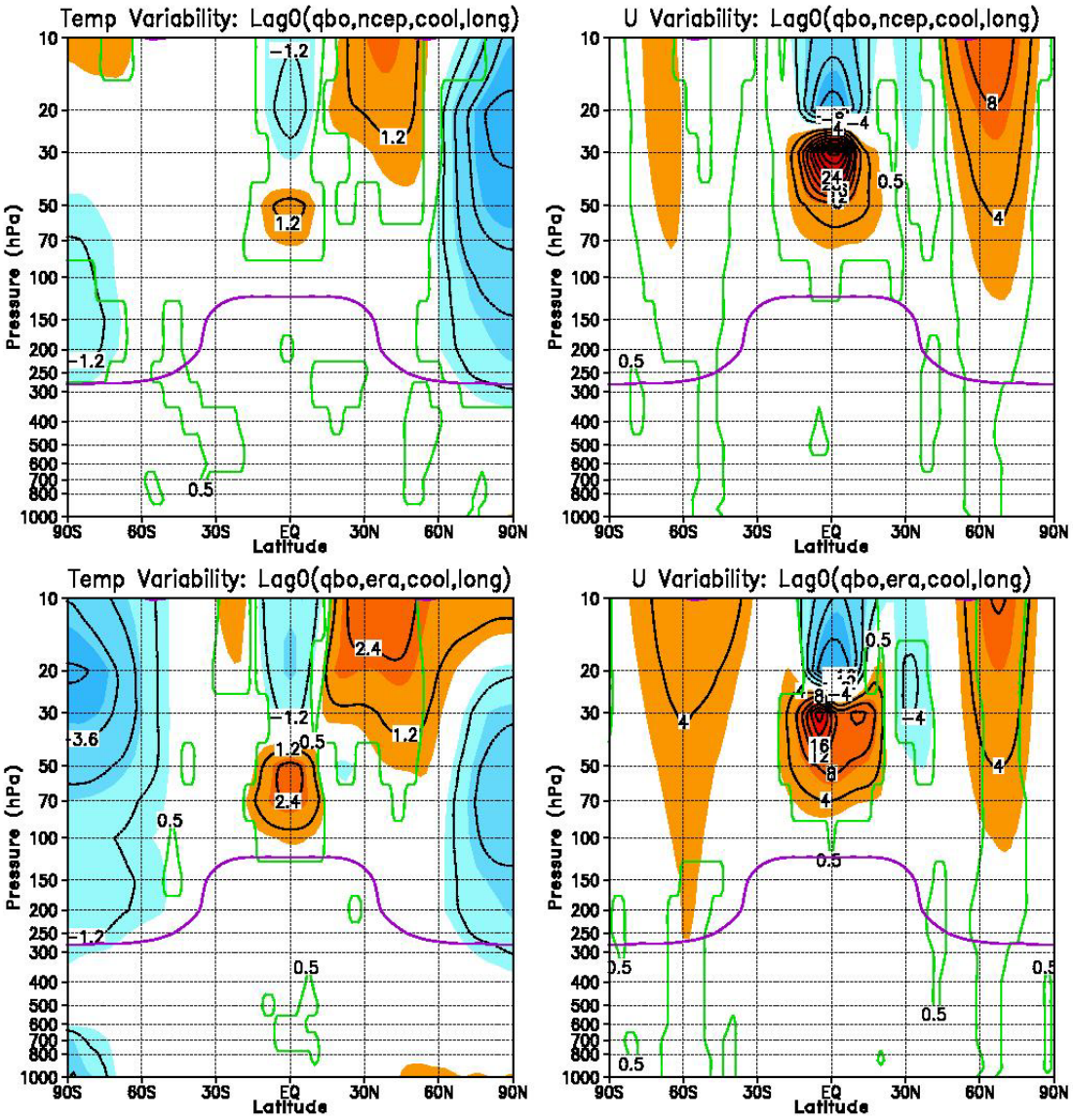

Figure 3.10. Variability in Temperature (left, K) and Zonal Wind (right, m/s) between maximum and minimum QBO index extremes during boreal cool seasons for the extended time period (1958-2001) in NCEP (top) and ERA 40 (bottom) reanalyses. Red (blue) shading indicates positive (negative) anomalies. Magenta contour indicates tropopause and green contours outline regions of significance of 95% or higher determined by a Student's T-test.

3.3 Solar Variability

The regressed zonal-mean temperature field reveals that variability in the 10.7cm solar flux can bring considerable temperature changes in both the NCEP/NCAR and the ERA datasets to the stratosphere and troposphere (illustrated in Figures 3.11. and 3.12). The complex structure revealed includes statistically significant warming in both the polar and subtropical lower stratosphere in the winter and summer hemispheres, evident in both datasets. The complex anomalous temperature field is matched by vertically banded structures in anomalous zonal mean winds due to thermal wind balance. These banded structures are illustrated in Figures 3.13 and 3.14.

The warming in the subtropical lower stratosphere is indicative of the high correlation between sunspot cycle and total ozone in the subtropics (Reid 1998). This warming is best illustrated in the NH after a four- to six- month lag after the maximum in the solar flux index. The ERA reanalyses reveals most clearly the slight tropospheric cooling directly below the subtropical lower stratosphere warming. The increase in static stability in the tropical troposphere reduces upwelling from the surface, lowering the tropopause, and subsequently weakening and shifting the subtropical jet poleward (Haigh et al. 2004). This is especially clear in the extended time period (Figure 3.15). In this extended period, zonal wind patterns in the SH are of opposite sign than those from the post-satellite time period, suggesting low confidence in reanalyses data in this region.

The regressed zonal-mean zonal wind field reveals a pattern associated with increased solar flux consistent through each case: anomalous easterlies at mid-latitudes, westerlies in the northern high latitudes, and westerlies in all of the tropical troposphere and lower stratosphere (Figures 3.13 and 3.14). This pattern compares well to Haigh et al. (2004) and is driven by the perturbation of thermal wind balance through an increased temperature gradient between the subtropics and high latitudes (Kodera and Kuroda 2002). Solar heating in the tropics expands the Hadley circulation, forcing the subtropical tropospheric jets to weaken and shift poleward, consistent with model

simulations by J. D. Haigh (2004). Labitzke (2000) shows that this tropospheric response is strongest in summertime, and is associated with enhanced Hadley circulation in both hemispheres.

It is possible that differences between the shortened time period and the extended period (as in Figure 3.15) may be explained by a change in atmospheric sensitivity to the solar flux, perhaps from an alteration in the background atmospheric chemical composition (Tinsley 2004). However, because there are considerable differences between the NCEP and the ERA 40 reanalyses in the extended time period, it seems that the most likely explanation is the considerable lack of data measurements before extensive satellite implementation in 1979.

Differences could largely be due to sampling issues. There are relatively few solar cycles that occur within the data record. In addition to this, sparser measurements of the equatorial stratosphere leave increased room for error (Baldwin 2004). The most dramatic anomalies are the polar warming and high latitude easterlies, consistent between datasets though not always significant. This pattern is inconsistent with existing theories of an enhanced stratospheric polar vortex. This motivates the incorporation of a general circulation model among other tools for a more thorough diagnostic study of the impact of solar variability.

SOL: Temperature Evolution in NCEP data over Cool Seasons (1979-2001)

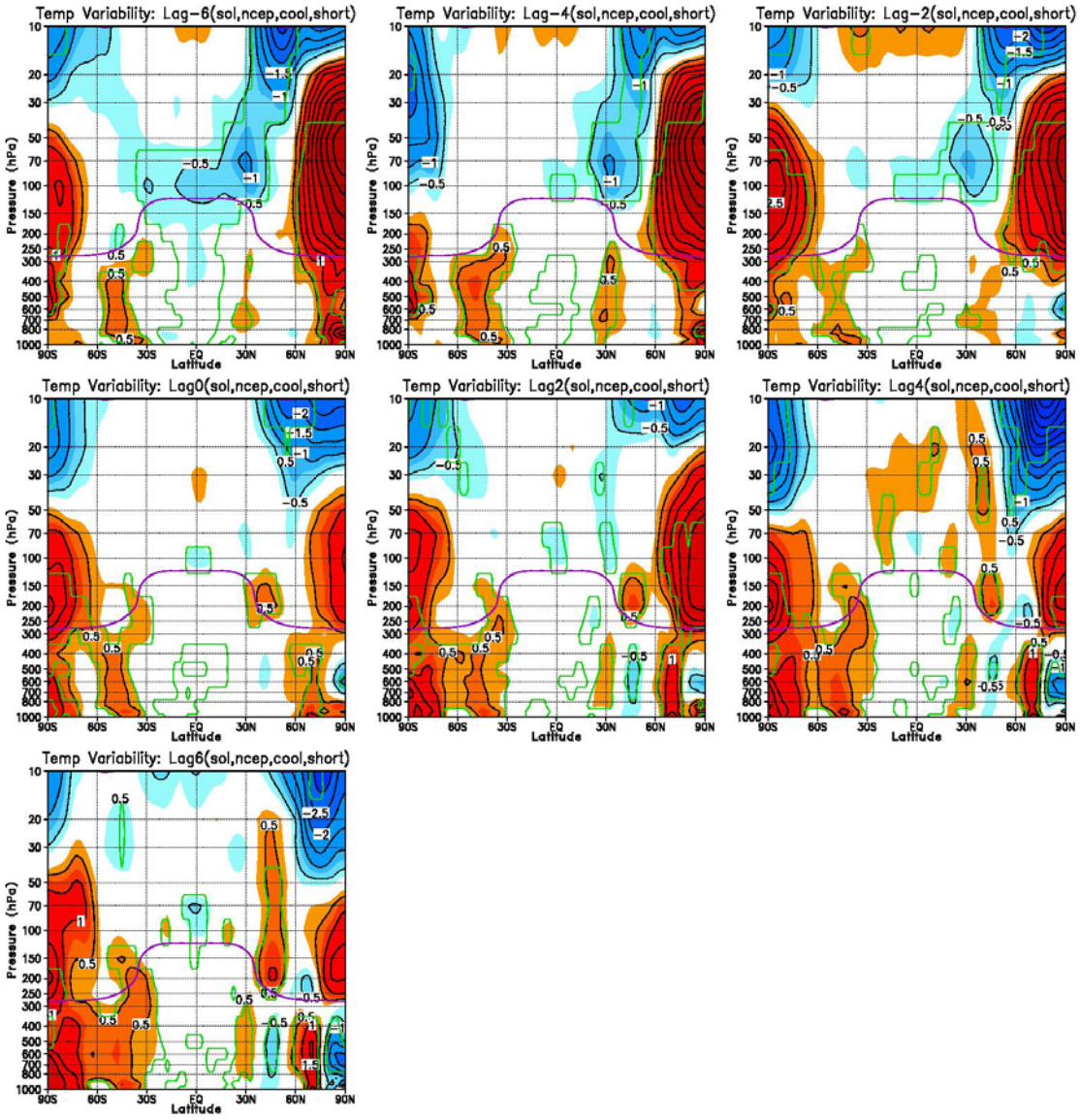

Figure 3.11. Variability between solar maximum and minimum in temperature (K) during boreal cool seasons (1979-2001) in NCEP reanalyses at 6 months prior through 6 months after index extremes. Red (blue) shading indicates positive (negative) anomalies. Magenta contour indicates tropopause and green contours outline regions of significance of 95% or higher determined by a Student's T-test.

SOL: Temperature Evolution in ERA data over Cool Seasons (1979-2001)

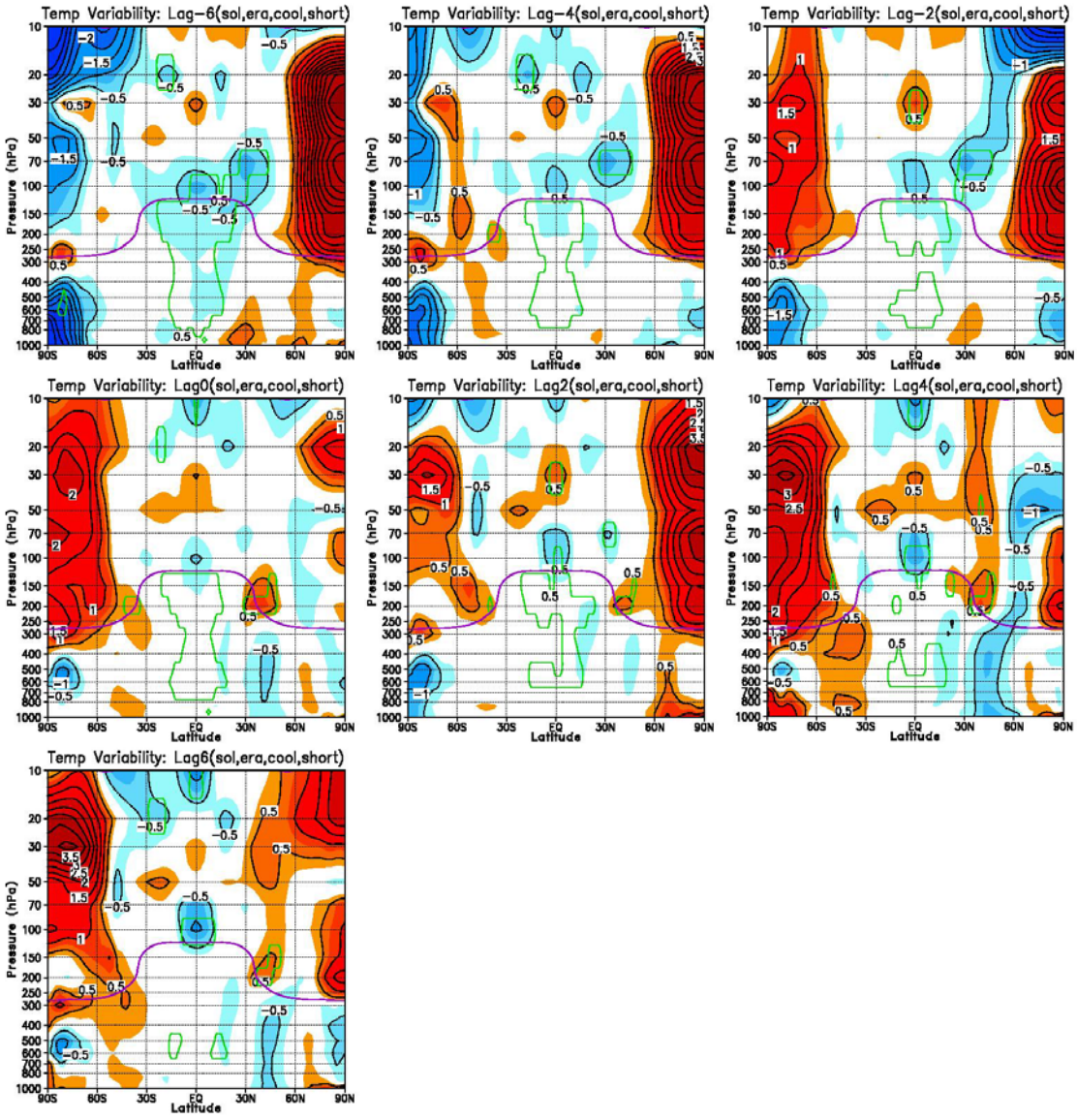

Figure 3.12. Same as Figure 3.11 except using ERA 40 data.

SOL: Zonal Wind Evolution in NCEP data over Cool Seasons (1979-2001)

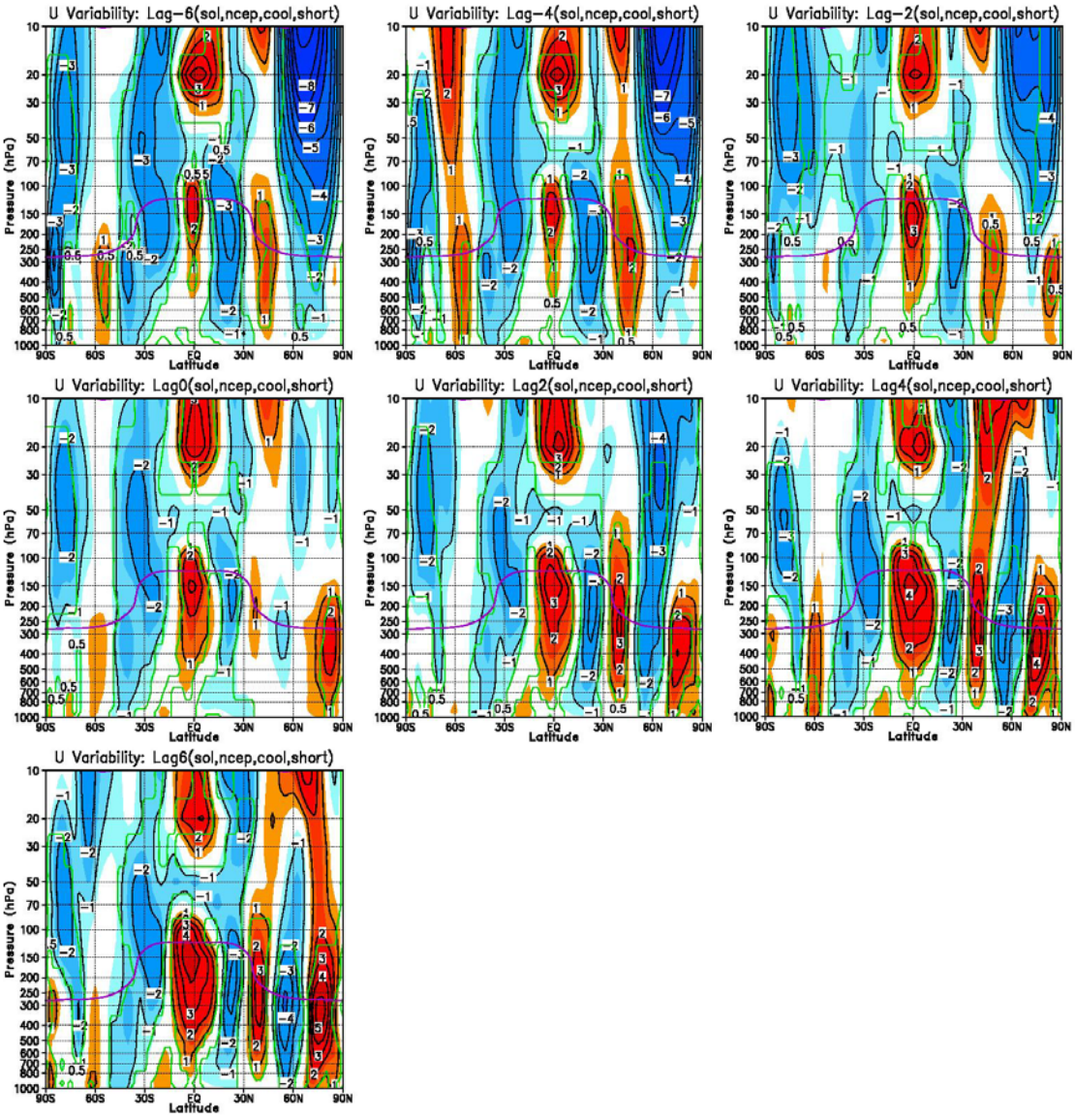

Figure 3.13. Same as Figure 3.11 except for Zonal Winds (m/s).

SOL: Zonal Wind Evolution in ERA data over Cool Seasons (1979-2001)

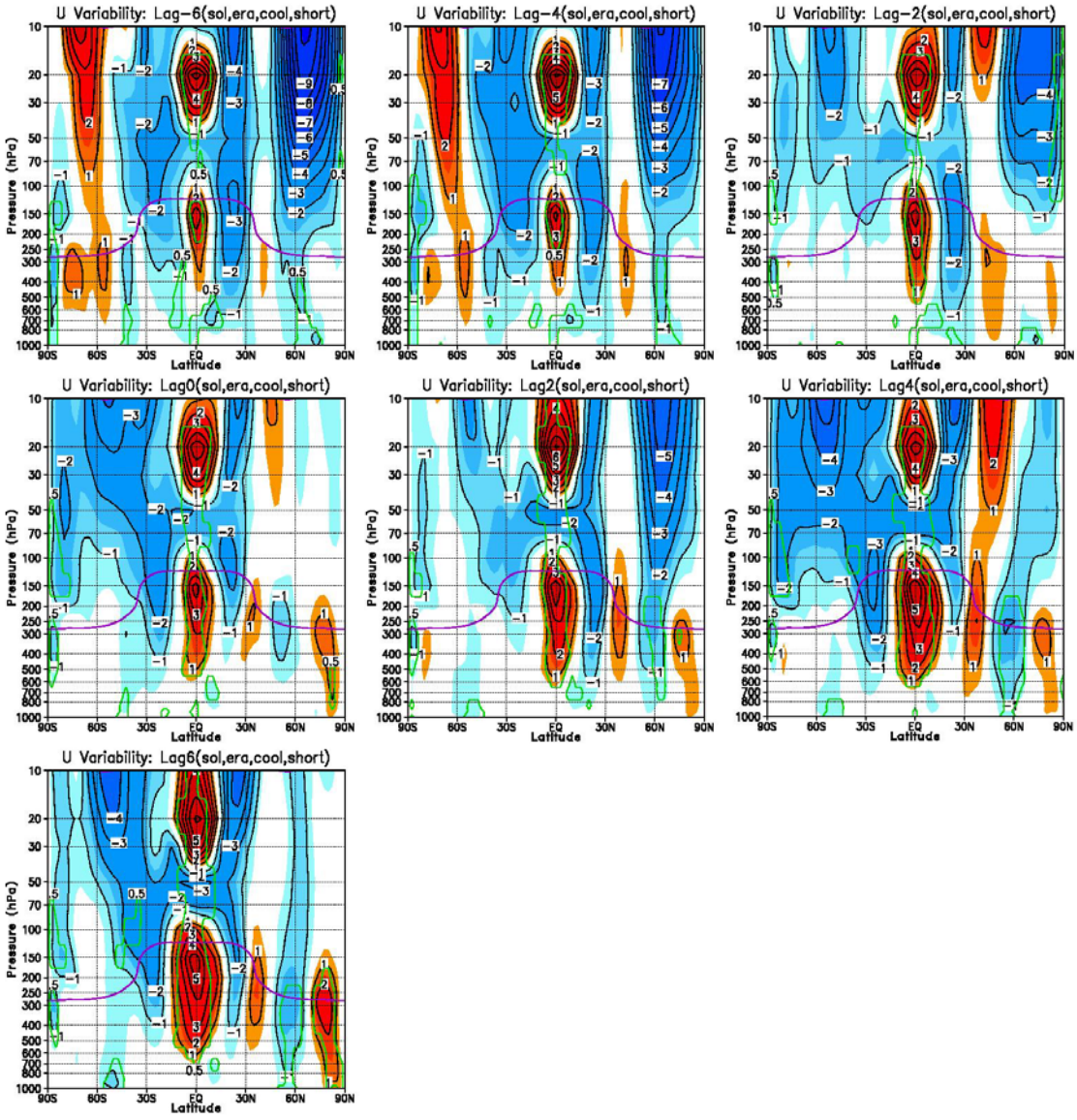

Figure 3.14. Same as Figure 3.12 except for Zonal Winds (m/s)**.**

SOL: Zonal Wind in NCEP and ERA during Cool Seasons

***Extended time Period* (1958-2001)**

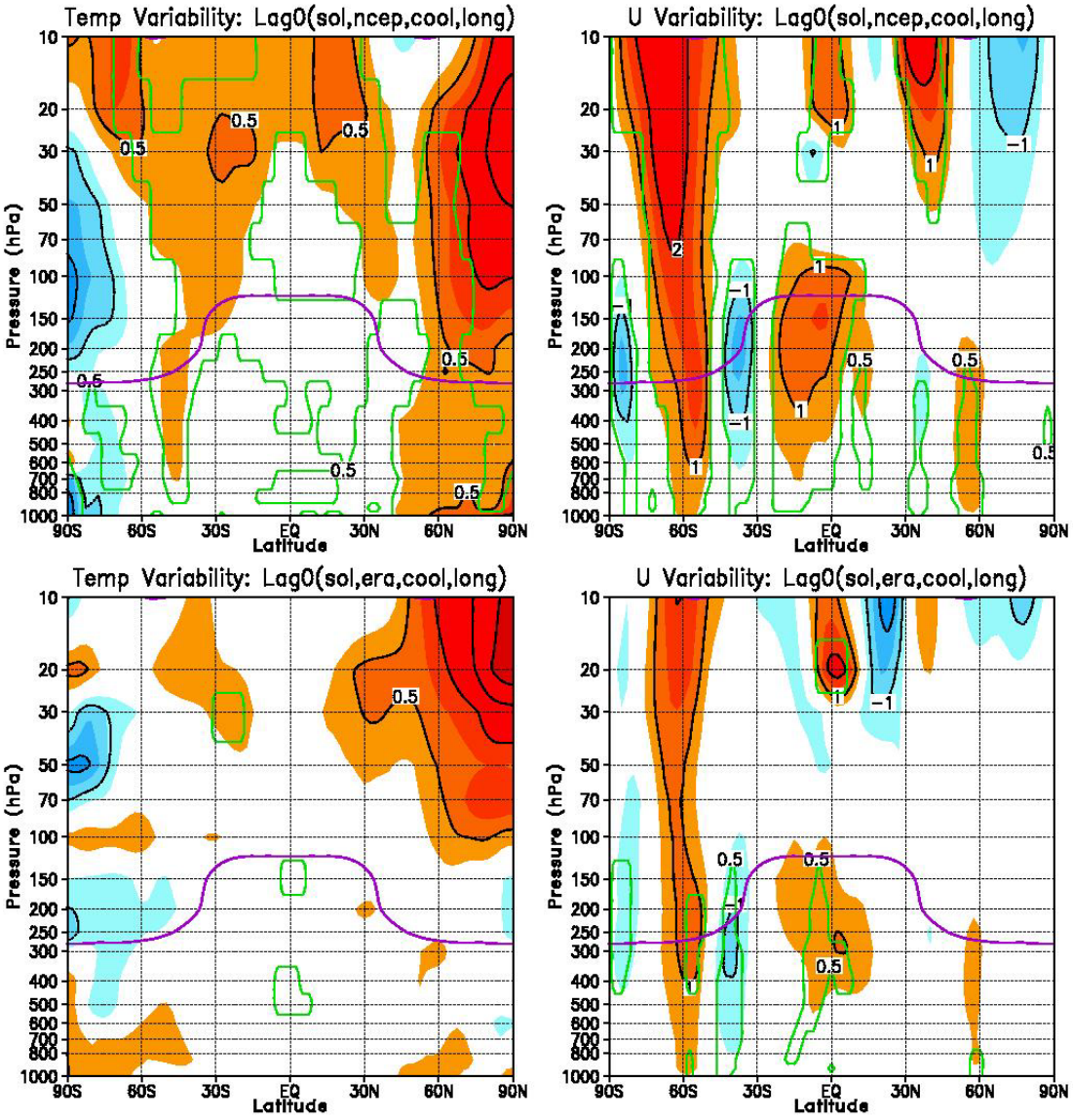

Figure 3.15. Variability between solar maximum and minimum index extremes in Temperature (left, K) and Zonal Wind (right, m/s) during boreal cool seasons for the extended time period (1958-2001) in NCEP (top) and ERA 40 (bottom) reanalyses. Red (blue) shading indicates positive (negative) anomalies. Magenta contour indicates tropopause and green contours outline regions of significance of 95% or higher determined by a Student's T-test.

3.4 Volcanic Activity

As discussed in the first chapter, the general scientific understanding of the atmospheric response to volcanic activity involves warming of the lower stratosphere due to radiative processes associated with stratospheric aerosol loading. This is evenly distributed in the summer hemisphere but is isolated to the equatorial region in the winter hemisphere. In winter, this results in an enhanced stratospheric polar vortex and increased vertical wind shear at the tropopause level. This reduces planetary wave propagation into the stratosphere, consistent with a positive AO response. Additionally, the troposphere undergoes widespread cooling due to increased stratospheric UV blocking. This study looks for consistency between this theory and observations during the boreal cool season. It is found that, while this pattern is not clear in the most recent data span (1979-2001), it does readily appear in the extended time span (1958-2001) when more observations of volcanic activity are incorporated.

Figures 3.16 and 3.17 illustrate the temperature difference between maximum and minimum stratospheric optical thickness through its temporal evolution (lags zero through 6 months) within NCEP and ERA reanalyses (respectively). In times of increased volcanic activity, both data sets reveal warming in the lower stratosphere at winter high latitudes. Inconsistencies between data sets include warming of the upper tropical stratosphere in NCEP data compared to a cooling in the ERA dataset. Activity within the SH reveals the largest dataset dependence. In general, the robust warming of the tropical lower stratosphere is not found. Figures 3.18 and 3.19 show the evolution of the zonal mean wind fields. Zonal wind profiles satisfy zonal wind balance, but indicate a consistent weakening of the stratospheric polar vortex. This does not agree with general scientific understanding of the climatic response to volcanic activity. However, in an investigation of the extended time period which includes more observations

volcanic eruptions, the expected warming in the tropical lower stratosphere is revealed, accompanied by an enhanced stratospheric polar vortex. Figure 3.20 illustrates these results using both NCEP and ERA datasets at high levels of significance (95% or higher within green contours).

VOLC: Temperature Evolution in NCEP data over Cool Seasons (1979-2001)

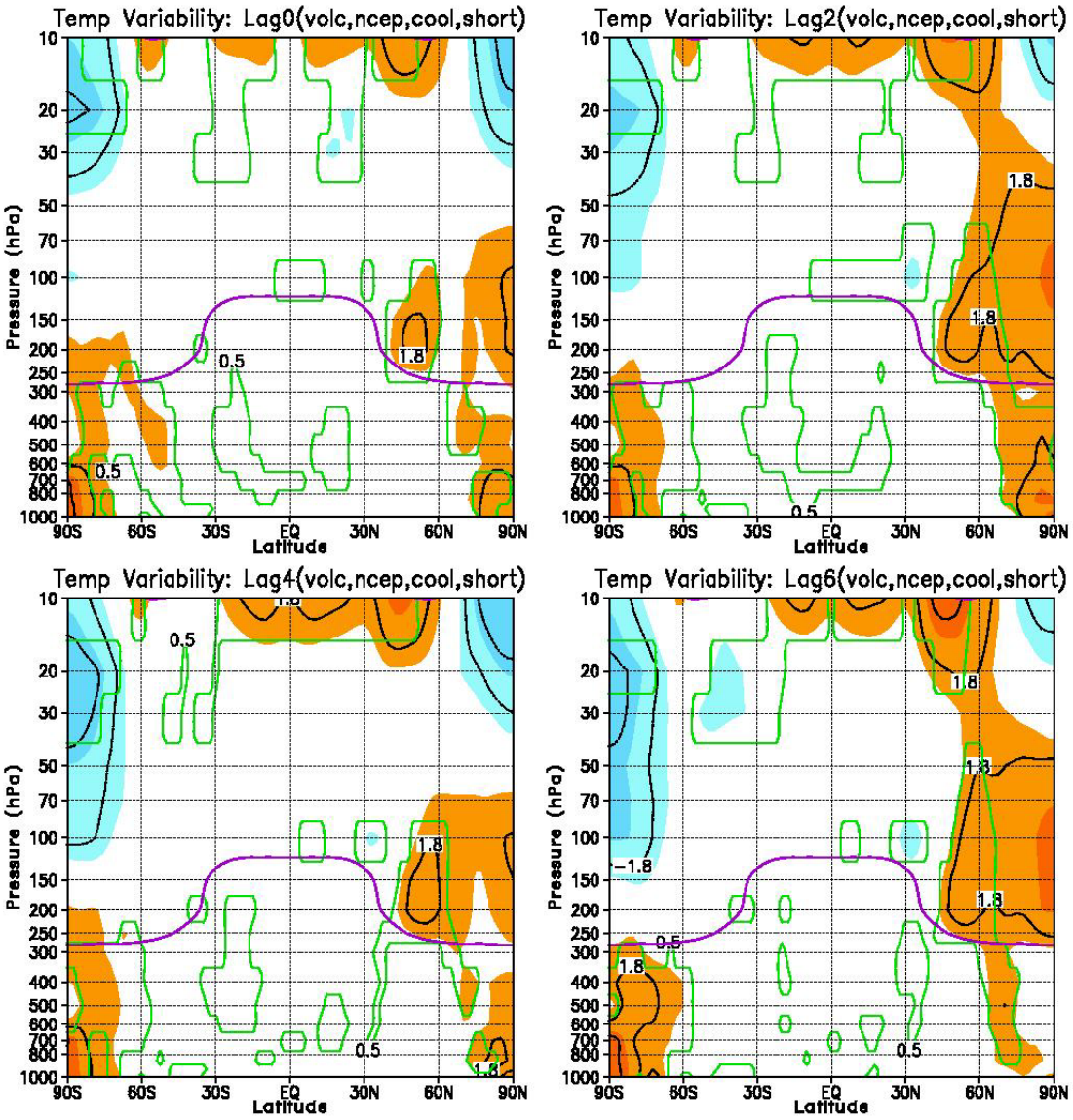

Figure 3.16. Temperature difference (K) between maximum and minimum of volcanic activity during boreal cool seasons (1979-2001) in NCEP reanalyses at index extreme through 6 months after index extremes. Red (blue) shading indicates positive (negative) anomalies. Magenta contour indicates tropopause and green contours outline regions of significance of 95% or higher determined by a Student's T-test.

VOLC: Temperature Evolution in ERA data over Cool Seasons (1979-2001)

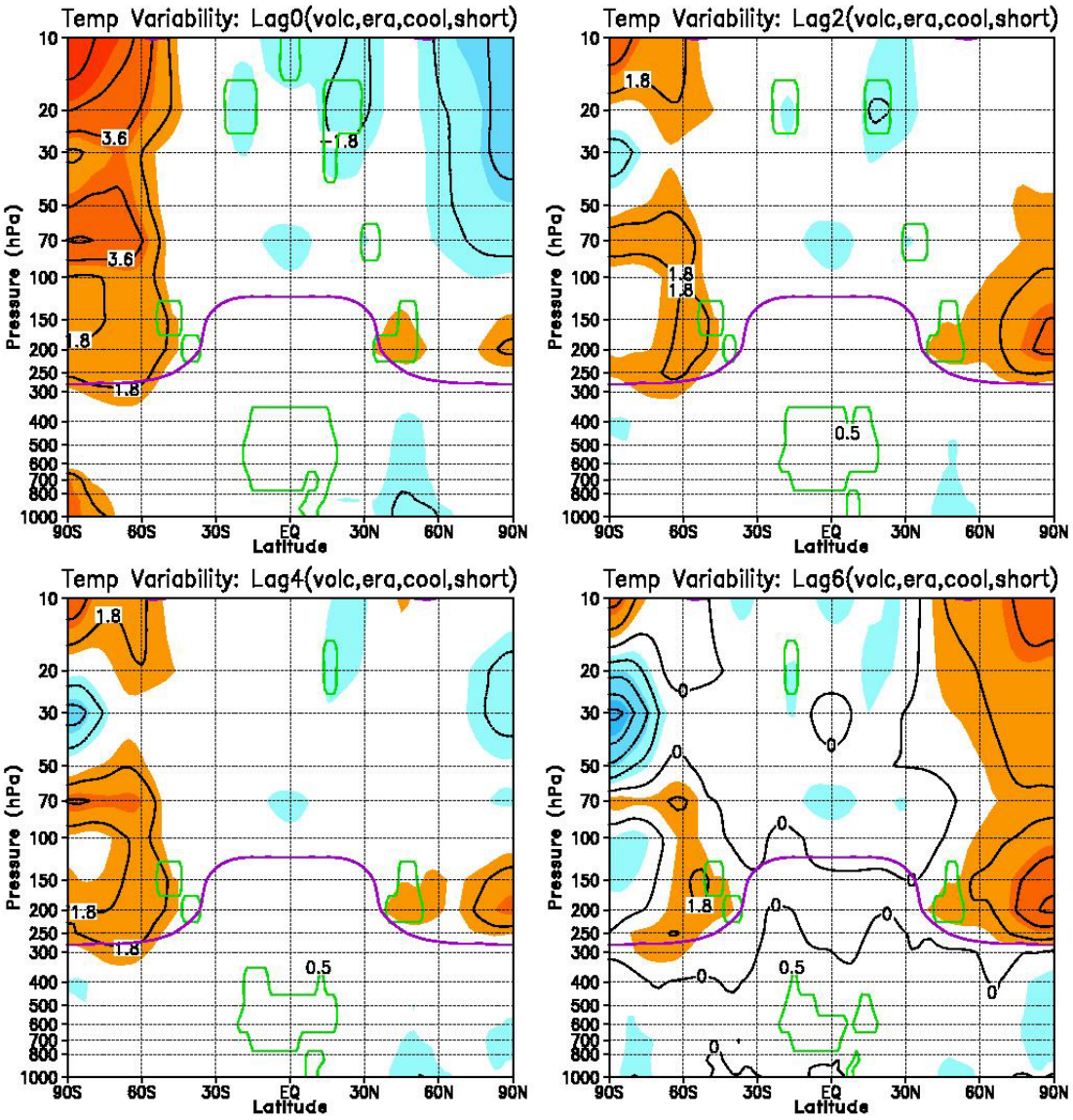

Figure 3.17. Same as Figure 3.16 except using ERA 40 data.

VOLC: Zonal Wind Evolution in NCEP data over Cool Seasons (1979-2001)

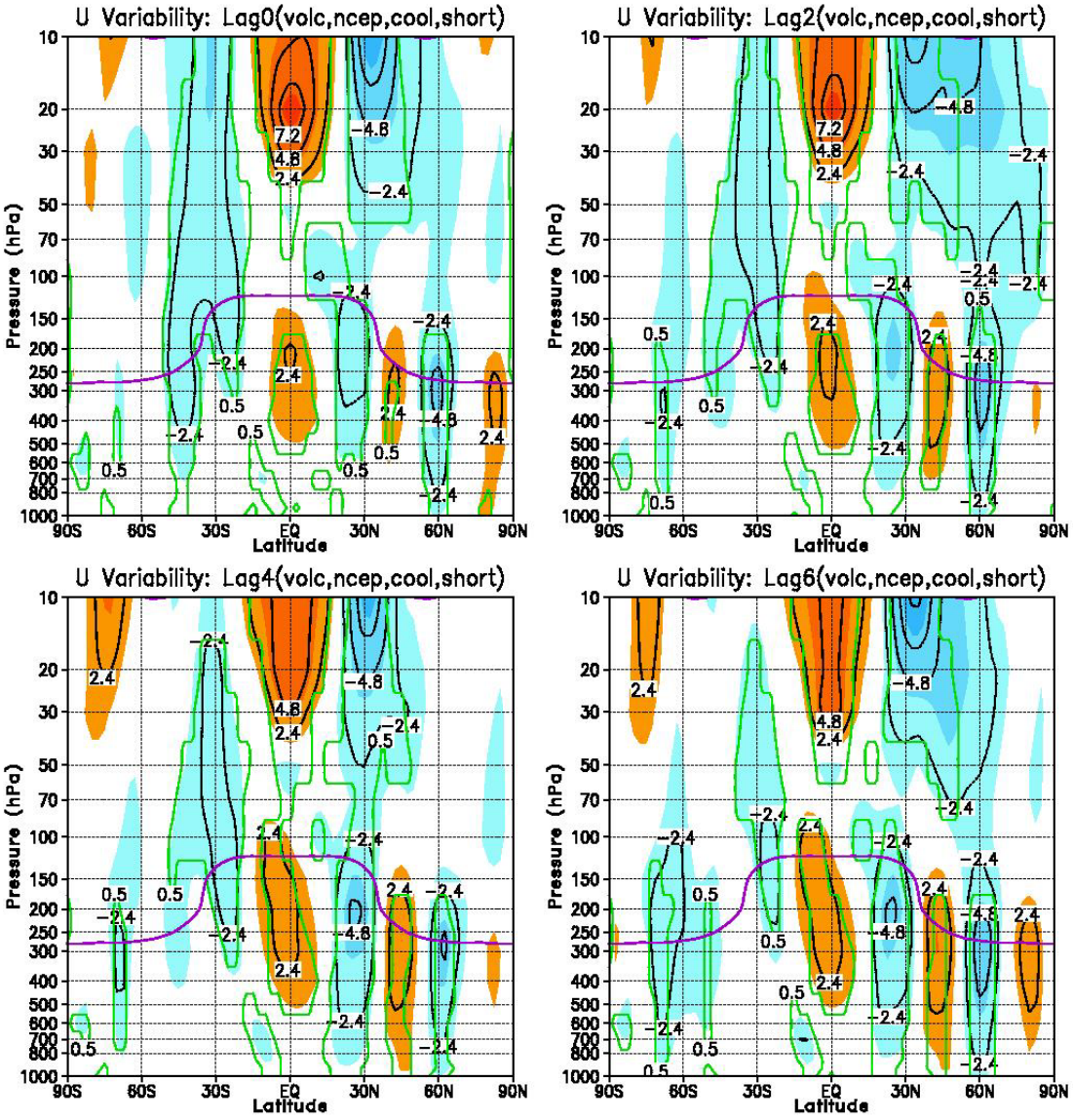

Figure 3.18. Same as Figure 3.16 except for Zonal Winds (m/s).

Zonal Wind Evolution in ERA data over Cool Seasons (1979-2001)

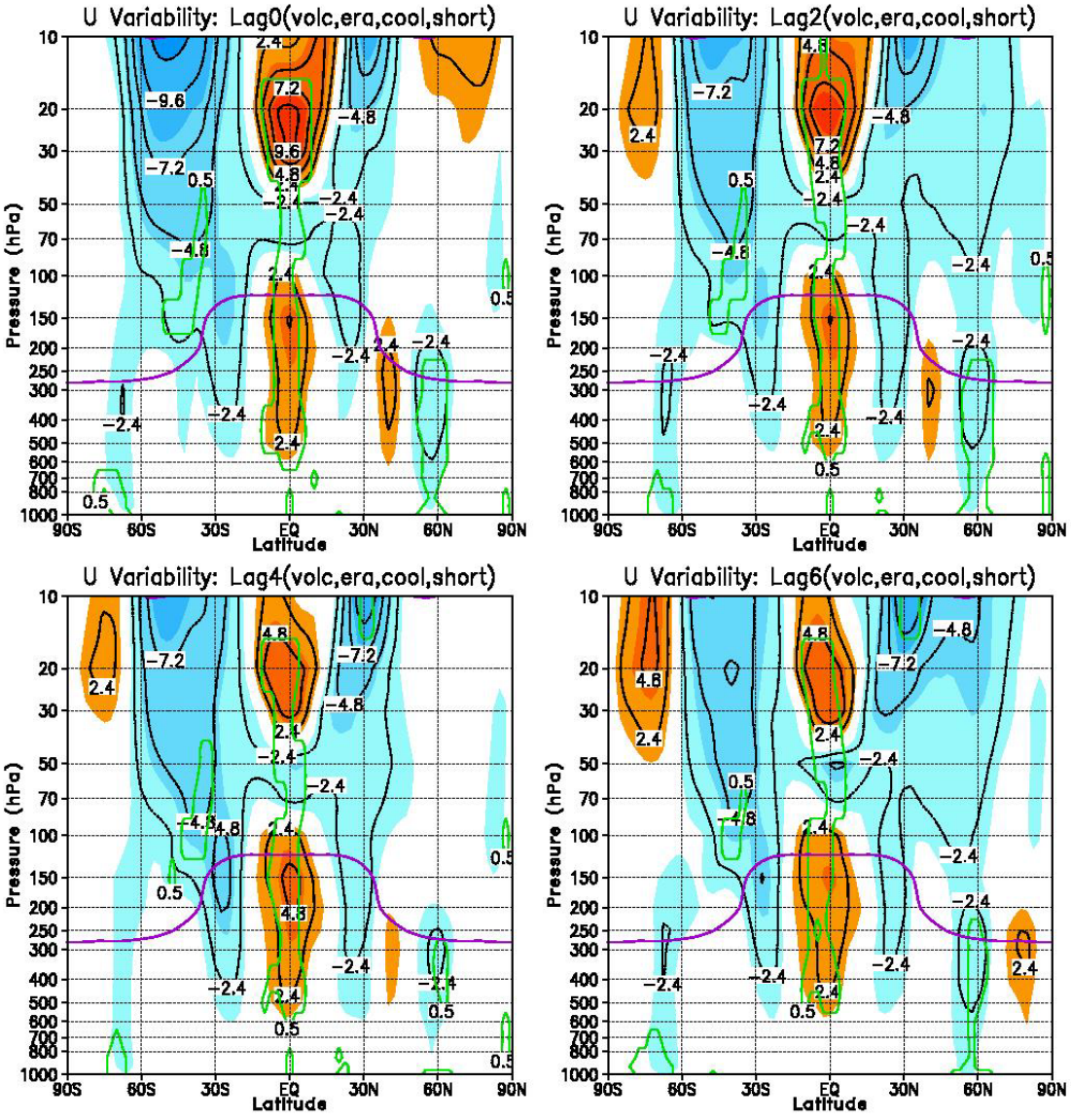

Figure 3.19. Same as Figure 3.17 except for Zonal Winds (m/s)**.**

VOLC: Zonal Wind in NCEP and ERA during Cool Seasons

***Extended time Period* (1958-2001)**

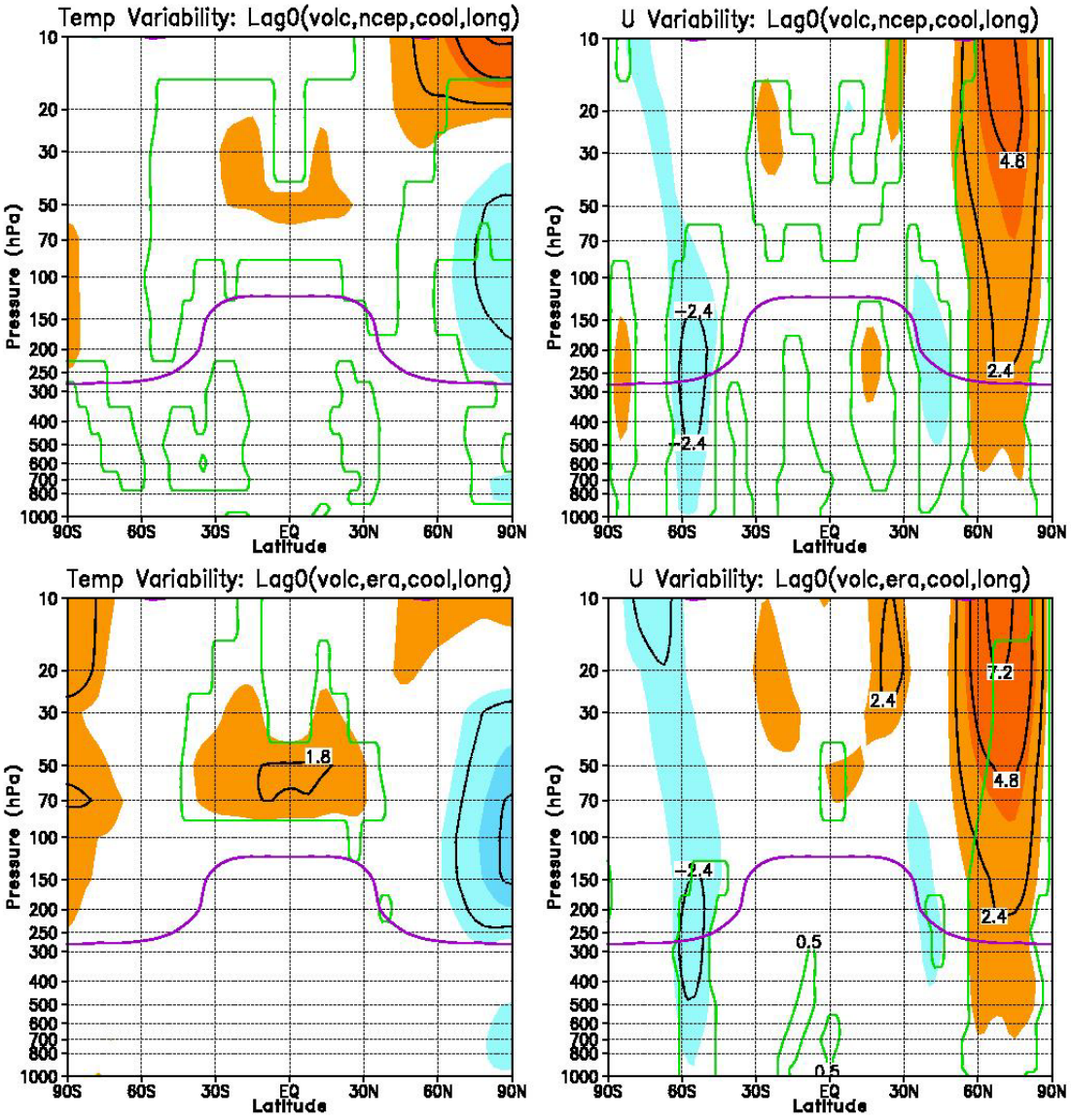

Figure 3.20. Variability in Temperature (left, K) and Zonal Wind (right, m/s) between maximum and minimum extremes of volcanic activity during boreal cool seasons for the extended time period (1958-2001) in NCEP (top) and ERA 40 (bottom) reanalyses. Red (blue) shading indicates positive (negative) anomalies. Magenta contour indicates tropopause and green contours outline regions of significance of 95% or higher determined by a Student's T-test.

CHAPTER 4

DIAGNOSTIC TOOLS

To assess the interaction between the stratosphere and troposphere in response to forcing of ENSO, QBO, solar variability and volcanic activity, the study is extended to incorporate four diagnostic tools: Eliassen-palm Flux/Wave driving analyses, Stream Function Analyses, Potential Vorticity Inversions, and employment of the Community Atmosphere Model GCM. For simplicity, we will continue our analysis with only the ERA reanalysis data set, considered to be the most thorough (Baldwin and Dunkerton 2004), and with focus placed on the NH.

4.1 Eliassen-Palm Fluxes and Wave Driving

Variability in anomalous EP fluxes (vectors) and associated wave driving (contours) between maximum and minimum in ENSO, QBO, solar activity, and volcanic activity during NH winters are presented in Figures 4.1 through 4.4, respectively. In the case of monthly eddy heat and momentum fluxes, the extended time period consists of data spanning from January 1958 through December 1997 and the post-satellite time period incorporates data from January 1979 through December 1997.

EP Vectors are scaled to account for aspect ratio and by inverse pressure to emphasize stratospheric values (each vertical and meridional component is multiplied by $e^{Z/H}$). Divergence of the EP flux is not preserved with this scaling but is implicitly represented in the wave driving, the net acceleration or deceleration of mean zonal wind due to large scale eddies (Baldwin, 1985). During the maximum in the ENSO index, enhanced vertical wave propagation in the stratosphere is observed as shown in Figure 4.1.

Though little significance was found for anomalous zonal wind fields in the northern extratropics associated with the QBO, one region of significance at the 95% level or higher can be accounted for by the wave driving analysis. At 60˚N, an enhanced westerly wind anomaly matches a zonal acceleration of the zonal mean wind illustrated in Figure 4.2. There is also evidence of the tropospheric wave propagation towards the equator just before and during the maximum westerly QBO winds, as shown in the EP Fluxes. This continues in the stratosphere slightly after the peak has been reached, leaving some indication of the zonal mean wind acceleration of the same sign as expected by the Holton-Tan effect.

Acceleration of the zonal mean winds within the polar regions of the troposphere (displayed in Figure 4.3) agree with the somewhat weak, but statistically significant acceleration revealed in the zonal mean wind observations (as previously noted in Figure 3.14). There is also an agreement between the theoretical prediction of waves being directed towards the equator during maximum in solar activity as seen clearly at midlatitudes in the troposphere for solar flux maximum. This is a possible indicator of stratosphere-troposphere coupling as waves are redirected within the troposphere because of suspected increased vertical wind shear, though a robust explanation is unclear. This perhaps is due to a reversal of meridional wave propagation as the jet moves northward during the span of winter. Anomalous meridional EP Fluxes have been shown to be poleward during the transition period, while more equatorward during the dynamically controlled period (Kodera and Kuroda 2002). The enhanced upward flux of Rossby waves in the stratosphere during solar maximum is also similar to other assessments (Zhou 2004).

Though the expected volcanically enhanced stratospheric vortex was observed only in the extended time period (1958-2001), expected evidence of the known mechanisms is observed in the EP flux and wave driving calculations. As seen in Figure 4.4, at the tropopause level in mid to high latitudes, an acceleration of the zonal mean

wind above 6 m/s is accompanied by divergent EP Fluxes in the same region. This involves a decrease in vertical wave propagation from the troposphere into the stratosphere as predicted by existing theory.

ENSO: EP Flux and Wave Driving Evolution

ERA data over Cool Seasons (1979-2001)

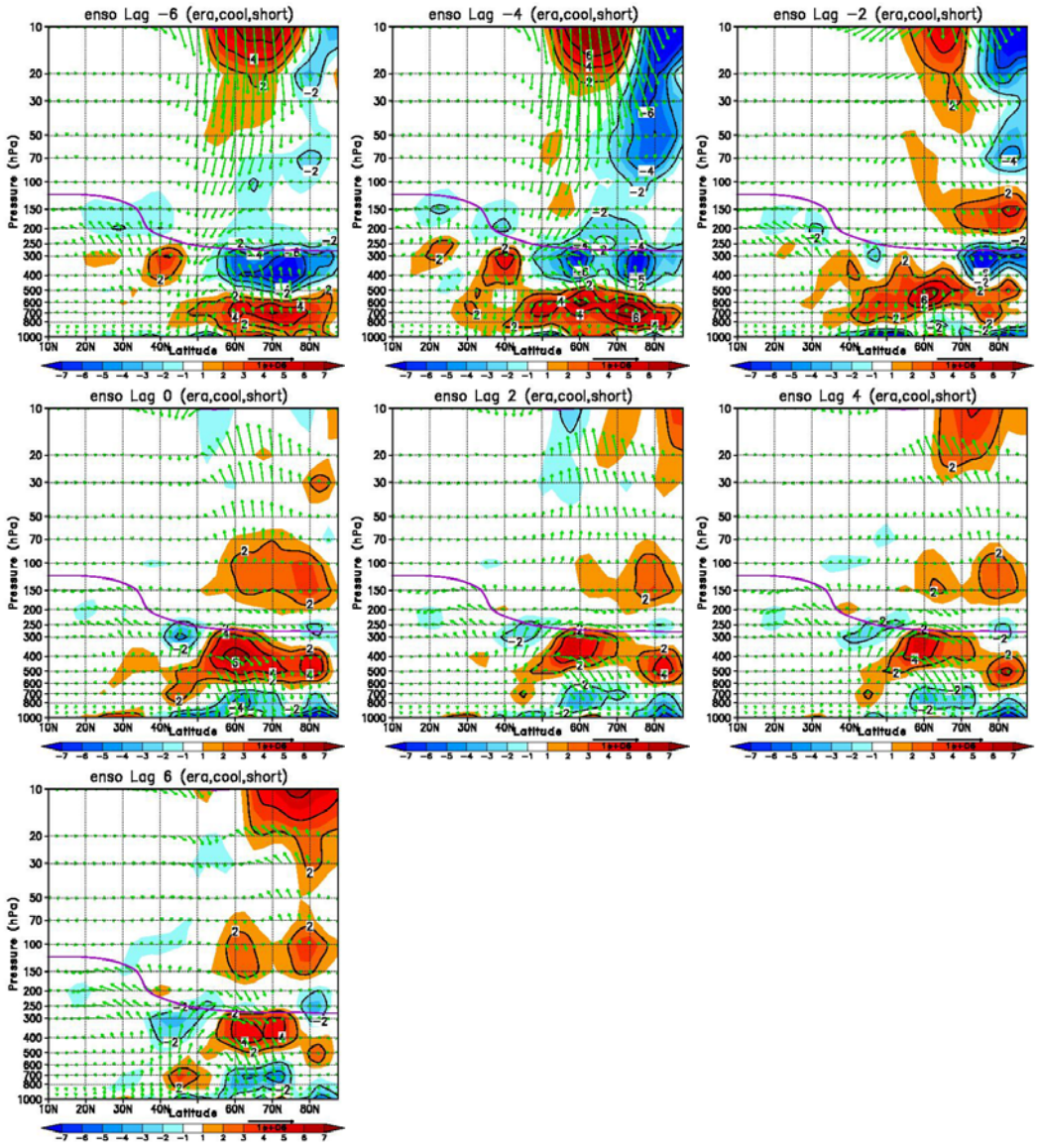

Figure 4.1. Variability between maximum and minimum ENSO in Eliassen-Palm Fluxes (Vectors) and Wave Driving (Contours, m/s/day) during boreal cool seasons (1979-2001) in ERA 40 reanalyses at 6 months prior through 6 months after index extremes. Red (blue) shading indicates positive (negative) anomalies. Magenta contour indicates tropopause.

QBO: EP Flux and Wave Driving Evolution

ERA data over Cool Seasons (1979-2001)

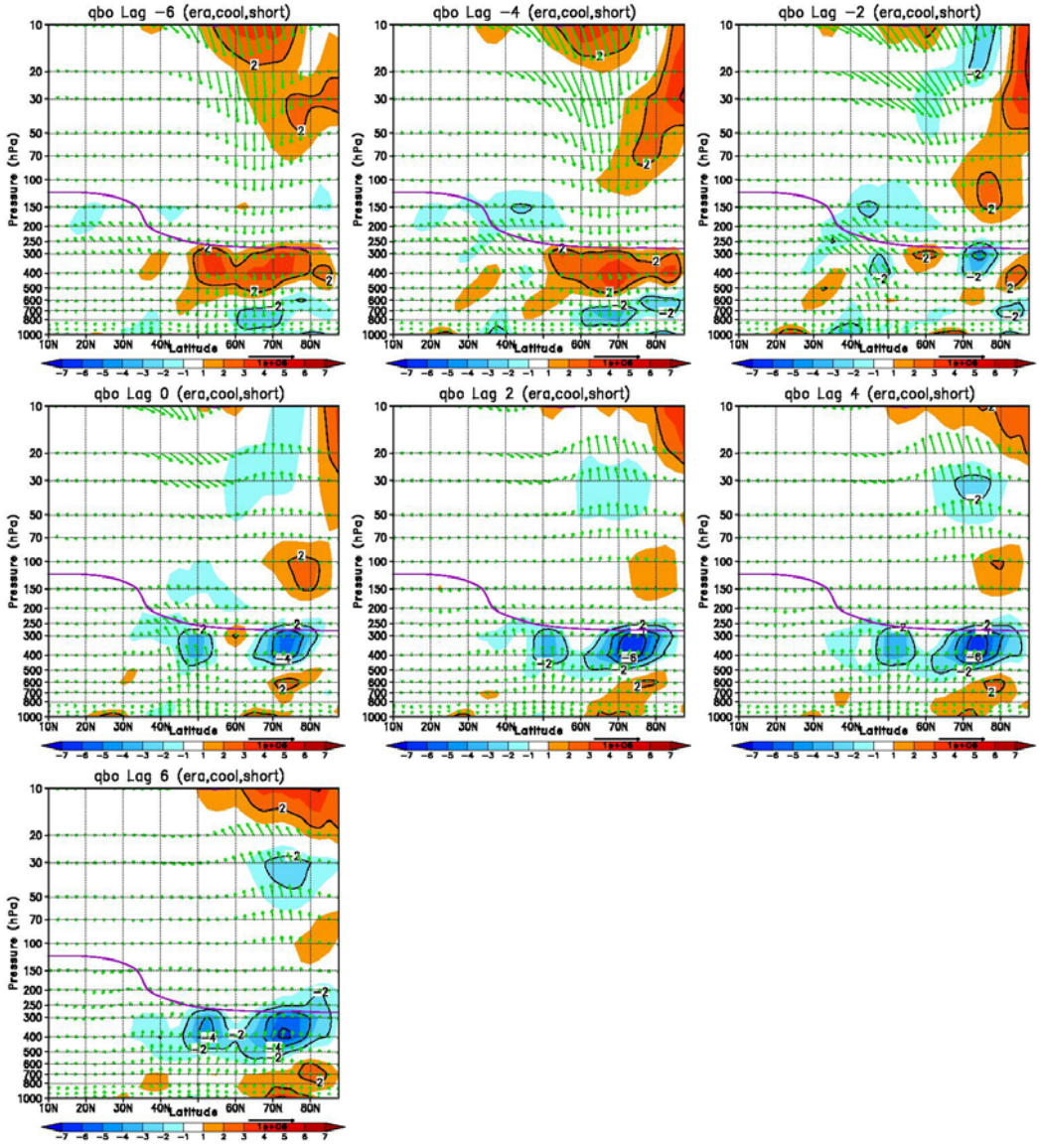

Figure 4.2. Same as Figure 4.1 except for the QBO**.**

SOL: EP Flux and Wave Driving Evolution

ERA data over Cool Seasons (1979-2001)

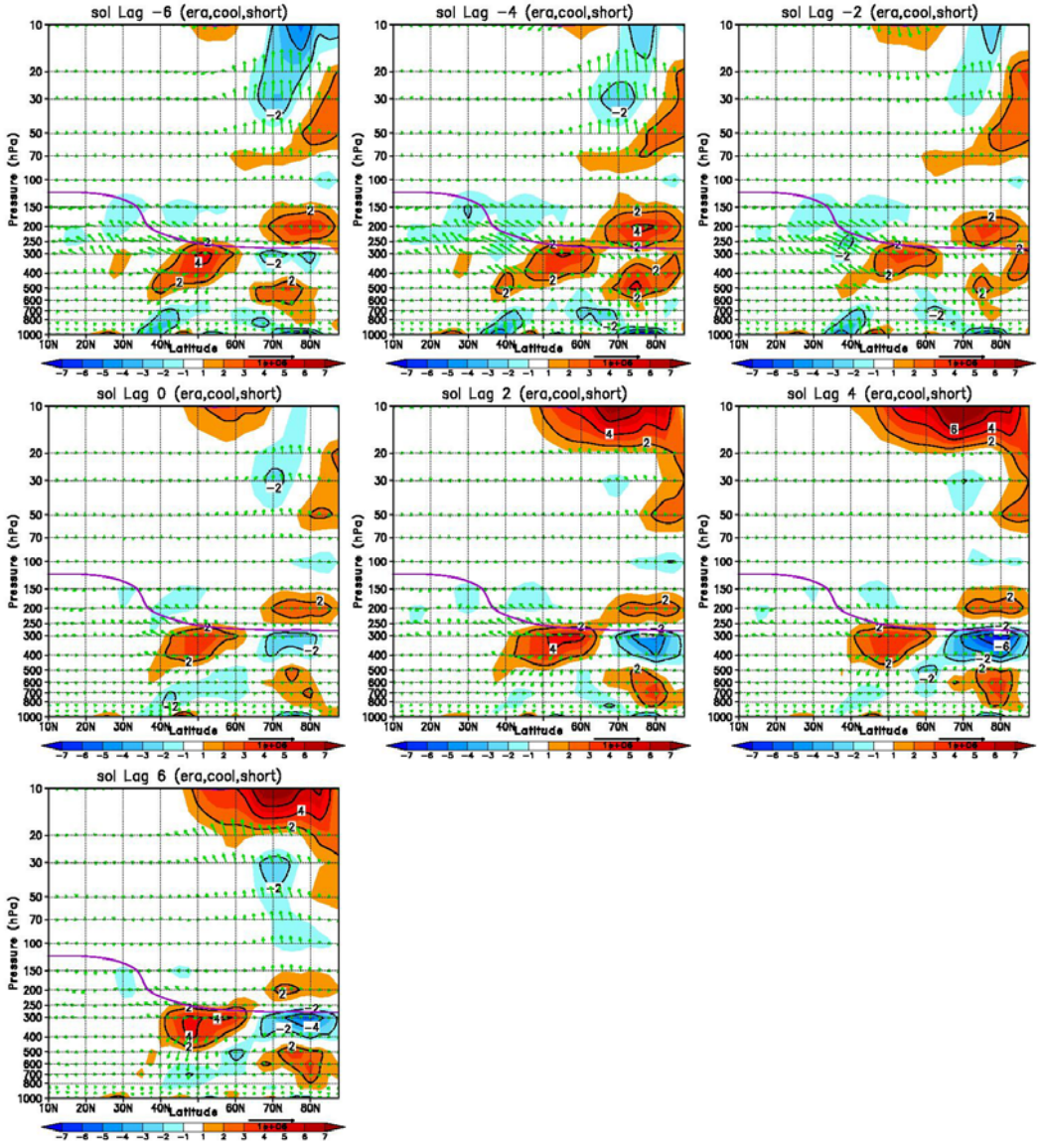

Figure 4.3. Same as Figure 4.1 except for Solar Variability**.**

VOLC: EP Flux and Wave Driving Evolution

ERA data over Cool Seasons (1979-2001)

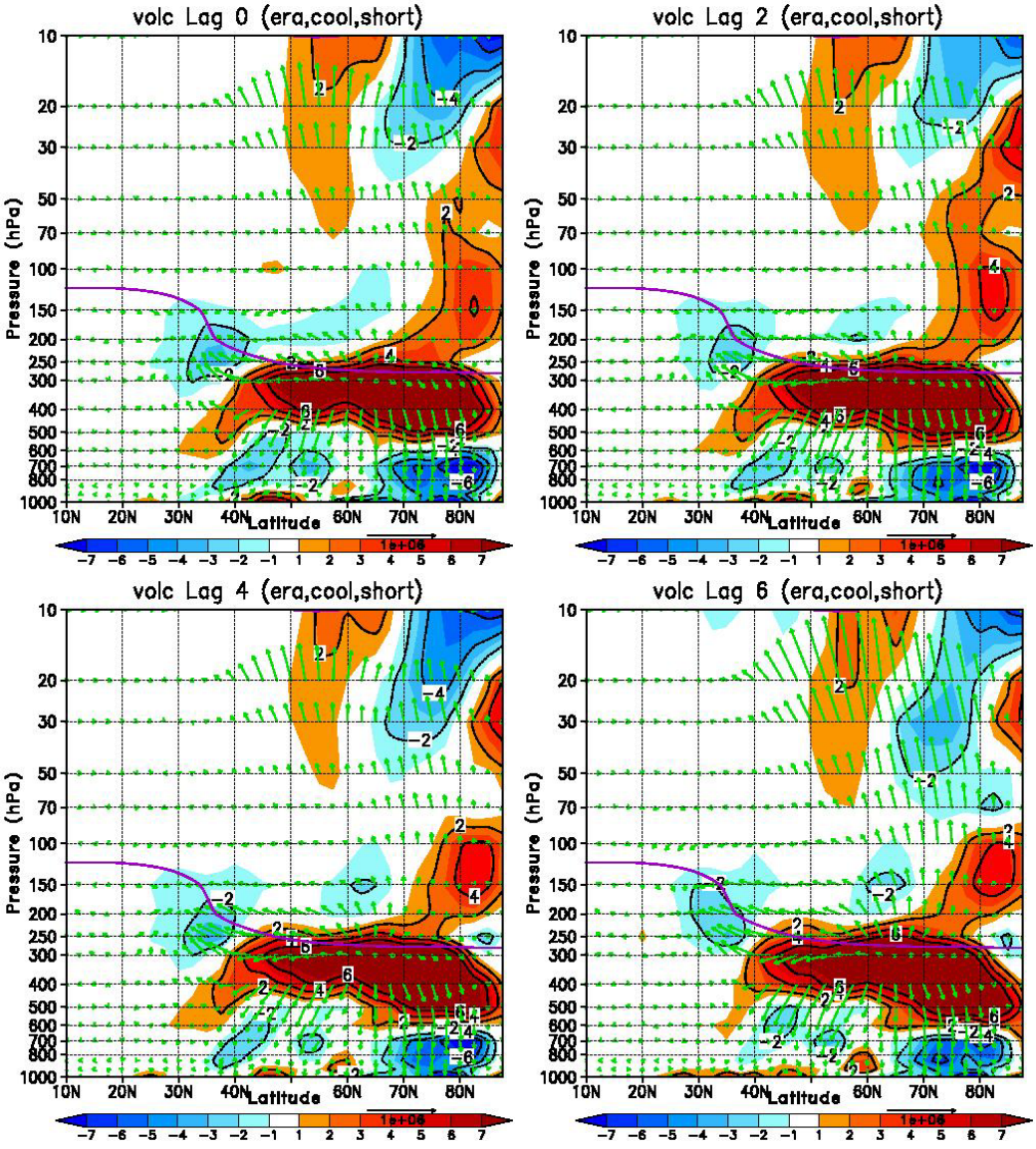

Figure 4.4. Same as Figure 4.1 except for volcanic activity. Lags zero through six months**.**

4.2 Stream Function Analyses

In an attempt to understand meridonal circulations induced by anomalous wave driving, stream functions analyses are performed with a particular focus on mid to high latitudes within the stratosphere. Plots of the NH wintertime anomalous meridional circulation within the ERA 40 dataset between maximum and minimum indices are illustrated in Figure 4.5.

During El Nino, the stream function analysis reveals anomalous poleward motion within the extratropical stratosphere (10 to 50 mb) followed by subsidence over the North Pole. The meridional circulation revealed is indicative of the downward control mechanism associated with enhanced wave breaking at this level. This is consistent with the general scientific understanding of enhanced wave propagation during the positive phase of ENSO. Additionally, complex structures result within the tropospheric Hadley circulation. Robust structures in the meridional circulation due to the QBO are not apparent within the stratosphere, but a weakening of the tropospheric Hadley circulation during the westerly phase of the QBO is indicated.

For both enhanced solar flux and enhanced volcanic activity, a weakened Brewer Dobson circulation is evident. This is a sign of reduced wave breaking within the stratosphere during maximum in solar and volcanic activity. Though the tropospheric signal is still complex, there is some indication of an enhancement of the Hadley circulation.

Anomalous Meridional Circulation

ERA data over Cool Seasons (1979-2001)

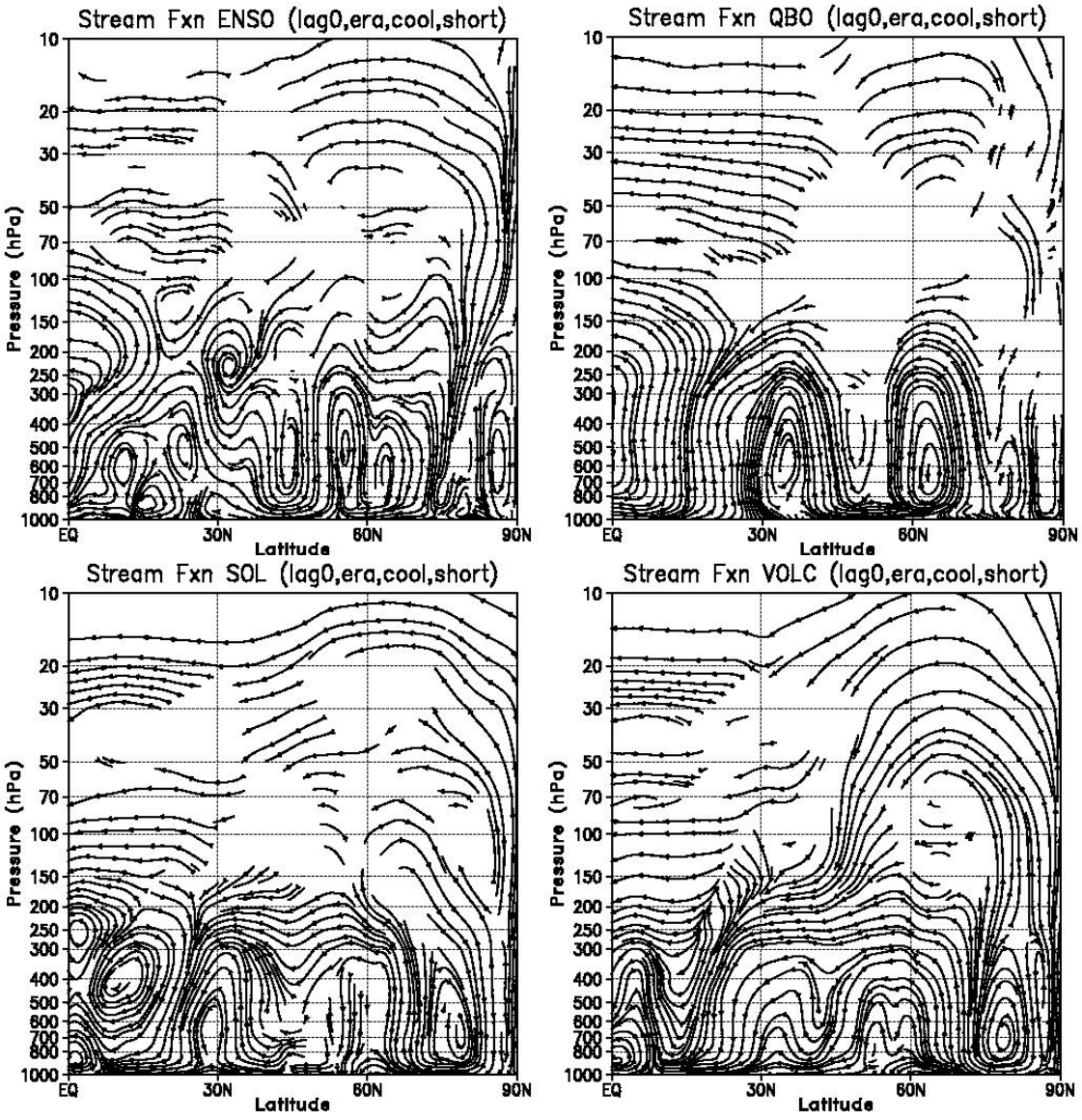

Figure 4.5. Anomalous stream function associated with modulation of ENSO, QBO, solar variability and volcanic activity during boreal cool seasons (1979-2001) in ERA ECMWF reanalysis.

4.3 Potential Vorticity Inversions

The PV equation (Equation 3) can be locally inverted using the piecewise PV inversion approach detailed in Black and McDaniel (2004) to identify remote sources of geostrophic zonal wind anomalies. In order to specifically assess the influence of stratospheric PV anomalies on the troposphere, the PV inversion technique is successively applied to the total PV field and the stratospheric PV field in isolation. The strongest latitudinal gradient in PV will be associated with the maximum anomalous zonal winds.

Variability in anomalous zonal mean winds associated with ENSO, QBO, solar variability and volcanic activity are displayed in Figures 4.6 through 4.9 (left panel), as previously discussed in chapter 3, now isolated to the NH. The induced anomalous geostrophic wind associated with the total PV fields are shown in the center panels. By comparing the results of inverting the full PV domain to the observed wind anomalies, it is clear that the PV inversion results reproduce the majority of the observed zonal wind anomalies in each case. Small differences between these two fields are associated with ageostrophic wind components not a produced by the PV inversion as well as boundary conditions. The center and right panels of Figures 4.6 through 4.9 may be compared to separate the zonal mean wind anomalies due to anomalous stratospheric and tropospheric PV fields. The right panels indicate variability in the zonal mean winds associated with anomalous stratospheric PV.

Variability in zonal mean winds associated with the ENSO forcing is apparent by contrasting center and right panels of Figure 4.6. Stratospheric PV anomalies account for most of the stratospheric circulation (a dramatic deceleration of the stratospheric polar

vortex) and have a significant impact on the tropospheric circulation in only the ERA reanalyses. Though the NCEP reanalyses (upper panels) reveal no substantial impact of the stratosphere on the troposphere, ERA reanalyses (lower panels) indicate that zonal mean winds are slowed throughout the depth of the extratropical troposphere during ENSO maxima. Another feature to note is that anomalous stratospheric zonal wind weakening is less intense once the impacts from the troposphere are included. This highlights another aspect of the stratospheric response to the troposphere.

Similar behavior is shown in Figure 4.7, where the response to anomalous tropospheric PV acts to weaken the impact of anomalous stratospheric PV within the stratosphere during the QBO. Though there is no robust indication of induced tropospheric zonal winds as a result of anomalous stratospheric PV, the statistically significant westerly acceleration between 50˚N and 60˚N along the tropopause is recreated using the PV inversion technique in the ERA reanalyses.

Solar variability results, illustrated in Figure 4.8, indicate that the banded structure of zonal mean winds originates partly from anomalous stratospheric PV fields but is reinforced by anomalous tropospheric PV. Though use of the NCEP reanalyses data (upper panels) reveals a robust response of tropospheric zonal mean winds to stratospheric anomalies, use of the ERA reanalyses data (lower panels) indicates no such response. This is a departure from the work of Baldwin and Dunkerton (2005) which found that more than half of anomalous surface pressure related to the solar cycle can be driven by wave forcing interactions within the stratosphere.

In the case of volcanic activity (Figure 4.9), results from the NCEP reanalyses (upper panels) reveal that half of tropospheric wind anomalies are induced by

stratospheric PV anomalies. This is not the case for the ERA reanalyses (lower panels). When expanded to the less reliable extended time series, one would expect results more consistent with the existing theories relating volcanic activity to interannual variability, simply from the fact that there was greater volcanic activity to observe within the extended time period.

Anomalous Zonal Wind Comparison: ENSO

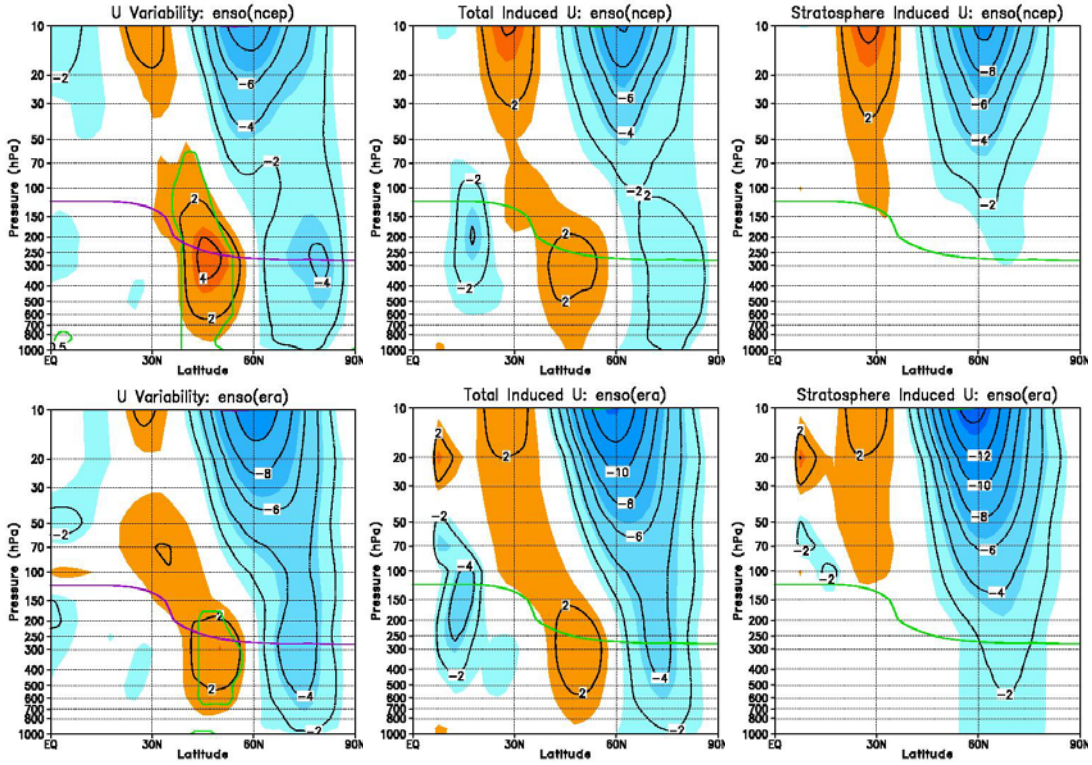

Figure 4.6. Variability in zonal mean wind (m/s) associated with ENSO. Left: As seen in Figures 3.1 and 3.2 at lag 0, but isolated to the NH. Center: Variability derived from the total PV anomaly field. Right: Variability derived from stratospheric PV anomalies. Upper panels use NCEP/NCAR ralanlyses. Lower panels use ERA reanalyses.

Anomalous Zonal Wind Comparison: QBO

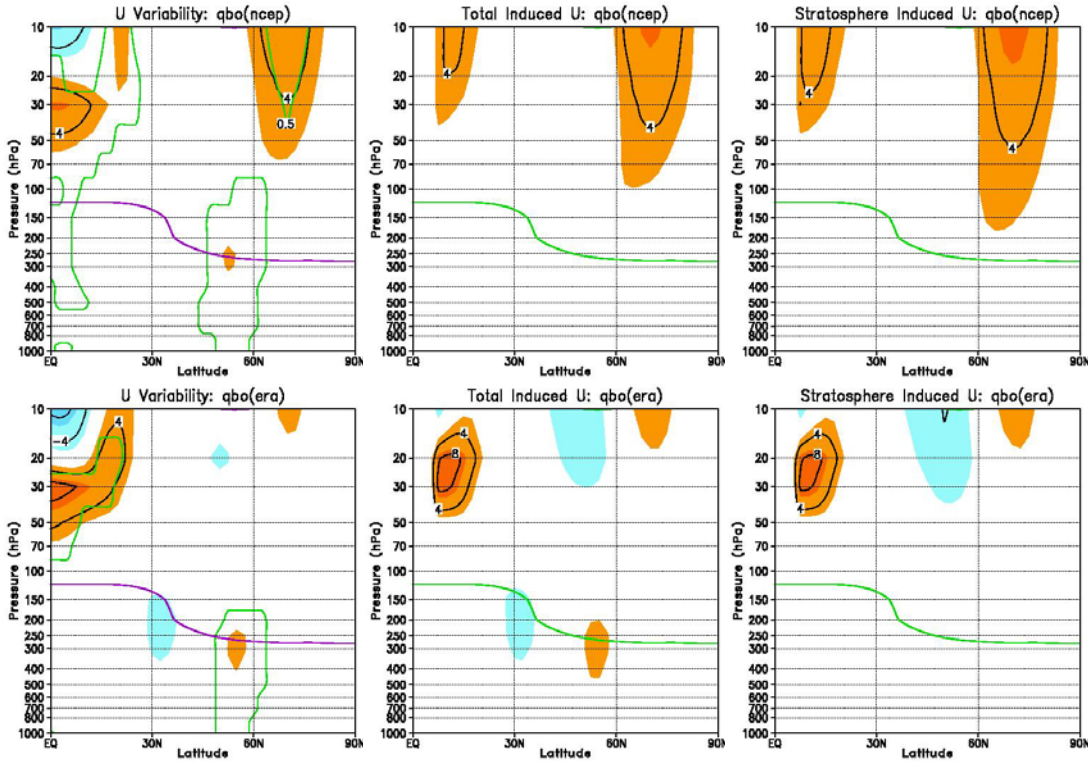

Figure 4.7. Variability in zonal mean wind (m/s) associated with QBO. Left: As seen in Figures 3.6 and 3.7 at lag 0, but isolated to the NH. Center: Variability derived from the total PV anomaly field. Right: Variability derived from stratospheric PV anomalies. Upper panels use NCEP/NCAR ralanlyses. Lower panels use ERA reanalyses.

Anomalous Zonal Wind Comparison: SOL

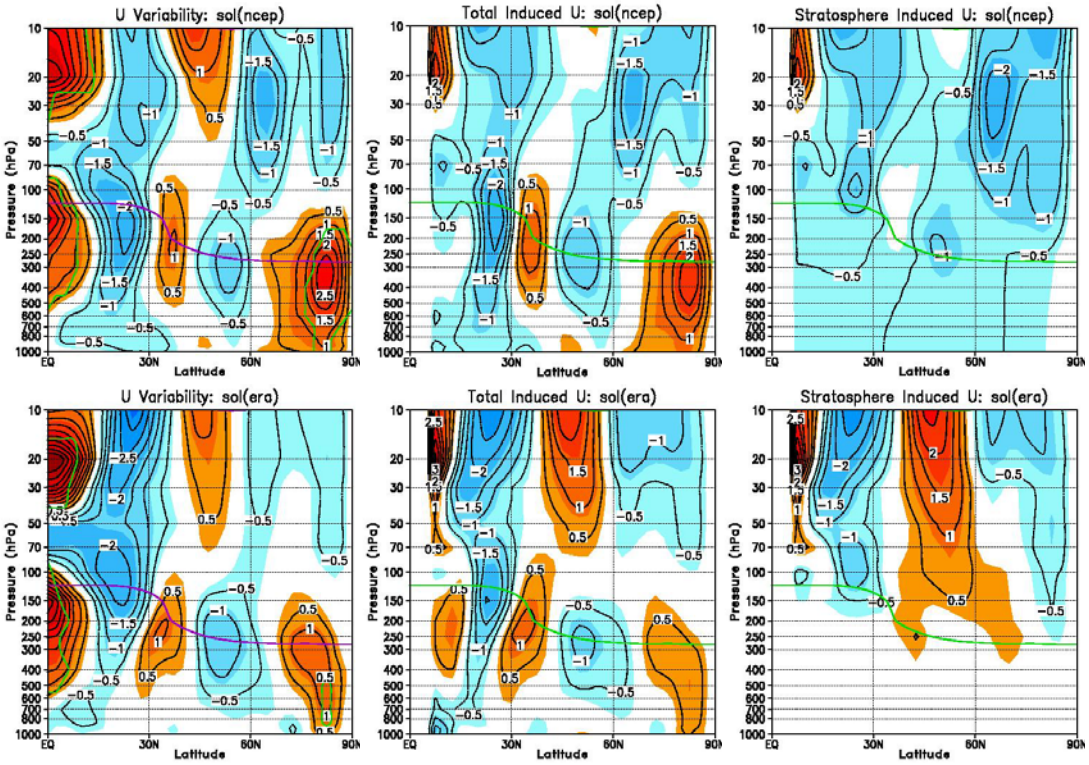

Figure 4.8. Variability in zonal mean wind (m/s) associated with Solar Activity. Left: As seen in Figures 3.13 and 3.14 at lag 0, but isolated to the NH. Center: Variability derived from the total PV anomaly field. Right: Variability derived from stratospheric PV anomalies. Upper panels use NCEP/NCAR ralanlyses. Lower panels use ERA reanalyses.

Anomalous Zonal Wind Comparison: VOLC

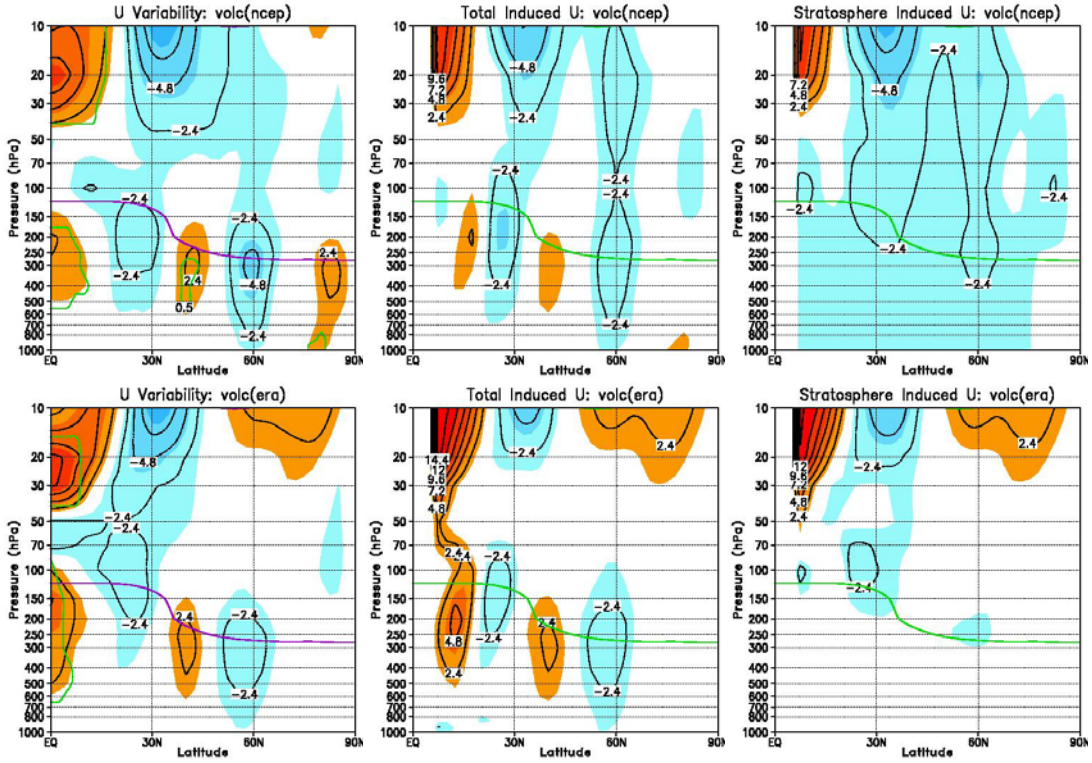

Figure 4.9. Variability in zonal mean wind (m/s) associated with Volcanic Activity. Left: As seen in Figures 3.18 and 3.19 at lag 0, but isolated to the NH. Center: Variability derived from the total PV anomaly field. Right: Variability derived from stratospheric PV anomalies. Upper panels use NCEP/NCAR ralanlyses. Lower panels use ERA reanalyses.

4.4 Model Simulation of Solar Activity

Simulations using a General Circulation Model (GCM) were performed to assess the impact of varied insolation because of inconclusive observational regression analyses of the influence of solar variability on the zonal mean circulation. The greatest benefit of using such a GCM is that nonlinearities may be better accounted for. However, a cautionary note is that the model is a simplified version of the atmosphere and thus has errors related to this simplification.

4.4.1 Varied Parameters

The GCM used in this study is the NCAR Community Atmosphere Model (CAM) 3.0 (McCaa 2004). The model simulated perpetual January conditions for five separate scenarios and a control case. Each case was selected to identify relationships between ozone levels, ultraviolet radiation (UV), total solar irradiance (TSI), and the dynamics within the atmosphere.

Table 4.1. Table of parameters increased in each case run.

Simulation Increases			
Case	Ozone	UV	TSI
1		√	
2	√		√
3	√	√	√
4	√		
5		√	√

In simulations with increased ozone, background concentrations of ozone initial conditions were raised 10% at the 5hPa level, with a logarithmic decrease above and below that level. In simulations with increased UV, constant incoming solar radiation in the ultraviolet band only (0.200 -0.245μm) was increased by 10%. In simulations with

increased TSI, total constant incoming solar radiation in all bands was increased by 0.1% (from 1366003 to 1367369 W/m^2). Combinations of these increases were included in cases one through five (detailed in Table 4.1), while the control case (case zero) had none of these increases.

4.4.2 Model Output

For each case, 50mb polar stereographic plots are presented for temperature (Figure 4.10) and zonal wind differences (Figure 4.11) from the control run. In addition, Figure 4.12 displays anomalies in Eliassen-Palm Fluxes and Wave Driving. All plots are derived using a 20 year average after model spin-up, the time needed for model to become balanced after initialization. As theory predicts, for many of the simulations, the temperature gradient is enhanced, the polar night jet is increased and there is an alteration of Rossby wave propagation associated with stratosphere-troposphere coupling.

As illustrated in Figure 4.10 for cases two through four, the temperature gradient in the NH is greatly increased with increase in initial ozone concentrations at the 5mb level. In cases one and five however, when only UV and TSI are increased, a somewhat opposite effect is observed indicating complexities of the ozone response. This may explain why case three, which has increases in all three parameters, is slightly weaker than cases two and four which do not alter incoming UV bands. Figure 4.11 shows similar plots for the anomalous zonal wind fields. From this, it is confirmed that regions of enhanced temperature gradients yield stronger westerly winds at mid to high latitudes in the stratosphere. Similarly, Figure 4.12 reveals that the greatest impact on the stratospheric zonal mean winds via wave driving occurs when ozone is increased (cases

two and four, with less of an impact in case three when changes in UV complicate the results). The acceleration of zonal mean winds at mid- to high latitudes near the tropopause is accompanied with equatorward propagation of planetary waves within the troposphere, consistent with current theories on stratosphere-troposphere coupling.

4.4.3 Implications

By comparison of these cases, it is clear that the response of ozone to incoming UV changes is complex, with a significantly different atmospheric dynamical response than evenly increasing ozone levels. However, the model simulation does indicate higher sensitivity to changes in the UV band than to a general increase in TSI. This is an expected result driven by ozone's specific dependence on incoming UV. The relationship is complicated by the dependence of ozone formation on stratospheric temperatures.

Model output from these five cases implies that there is an atmospheric response to solar variability that is not captured by current observations due to data limitations and the low signal to noise ratio. Theory suggests a significant atmospheric response to the low frequency forcing of solar variability, which model simulations support. Evidence of this in both the NCEP and ERA reanalyses datasets is not robust, exposing limitations in the use of such data for climatic research of this nature.

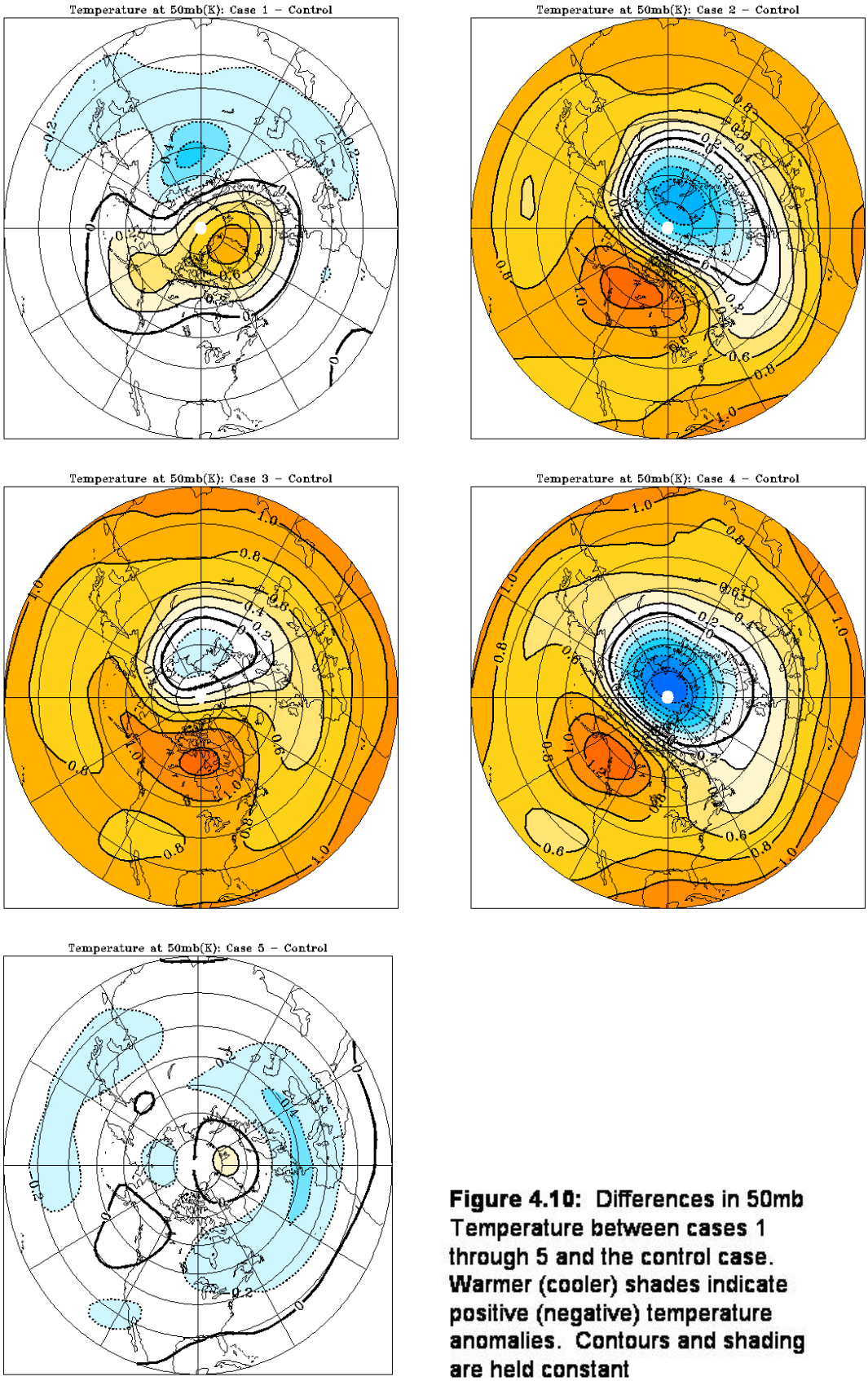

Figure 4.10: Differences in 50mb Temperature between cases 1 through 5 and the control case. Warmer (cooler) shades indicate positive (negative) temperature anomalies. Contours and shading are held constant

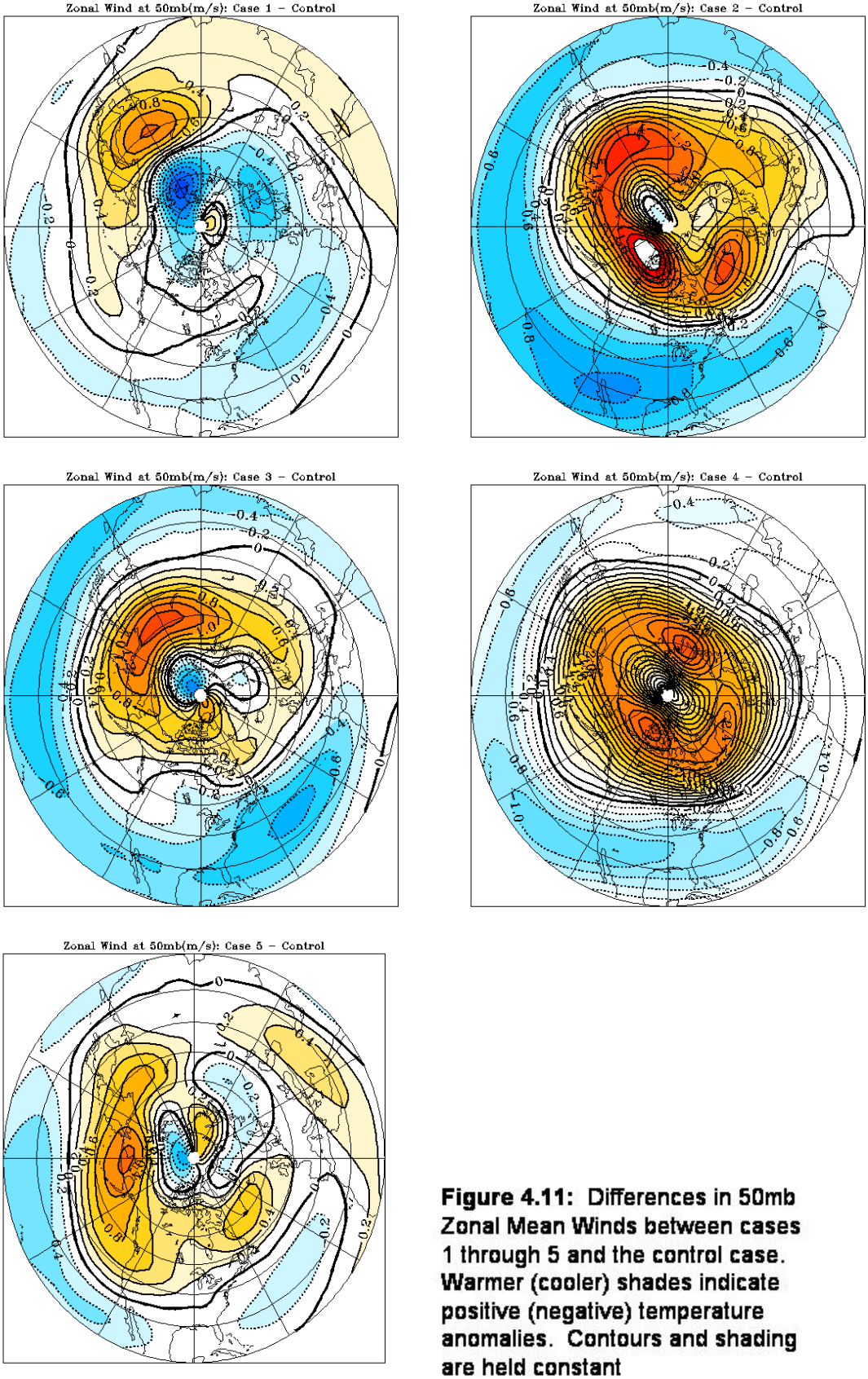

Figure 4.11: Differences in 50mb Zonal Mean Winds between cases 1 through 5 and the control case. Warmer (cooler) shades indicate positive (negative) temperature anomalies. Contours and shading are held constant

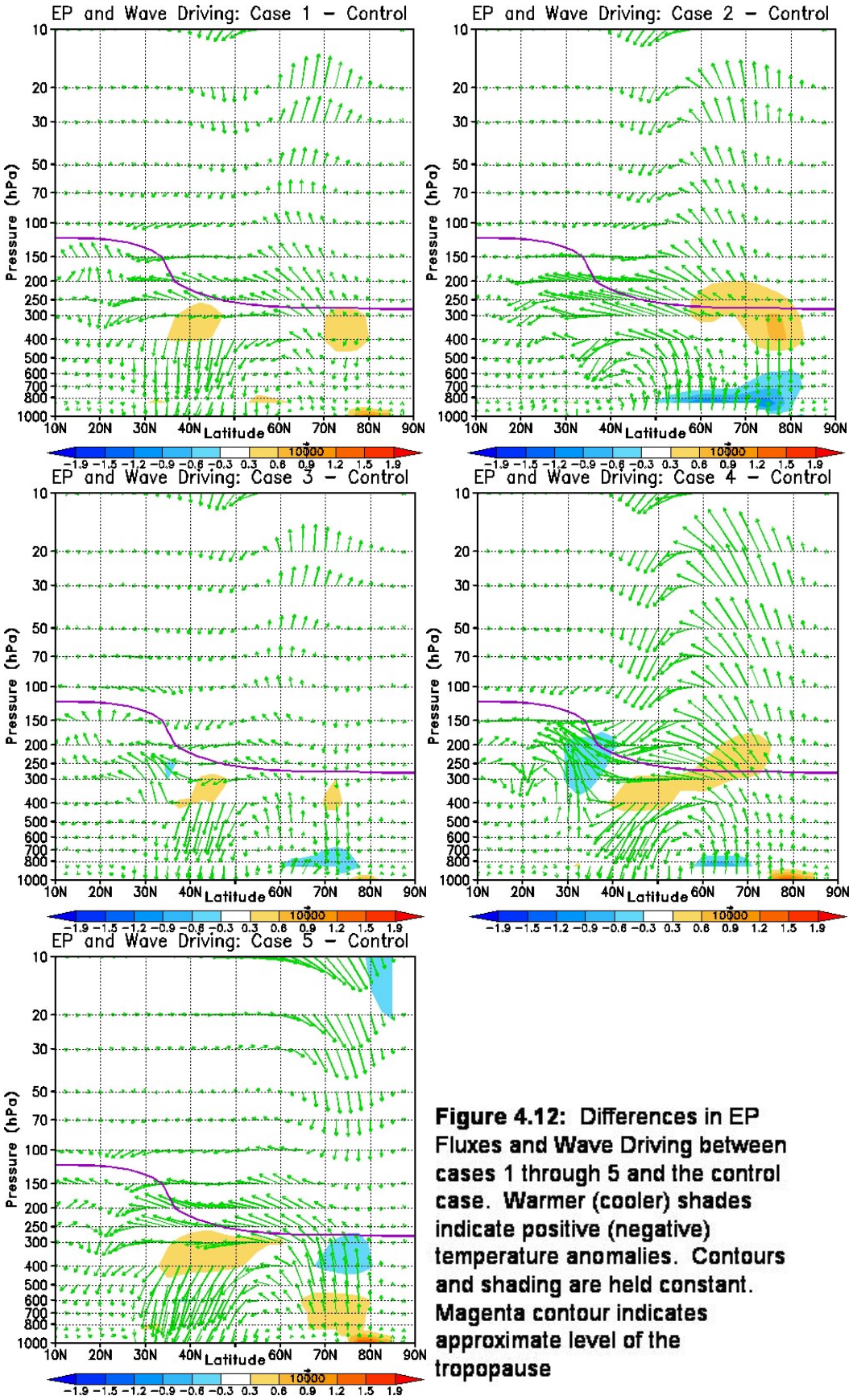

Figure 4.12: Differences in EP Fluxes and Wave Driving between cases 1 through 5 and the control case. Warmer (cooler) shades indicate positive (negative) temperature anomalies. Contours and shading are held constant. Magenta contour indicates approximate level of the tropopause

CHAPTER 5

DISCUSSION

In this study, an attempt was made to isolate signals of interannual variability associated with the El Nino Southern Oscillation, the Quasi-Biennial Oscillation, the 11-year solar cycle, and volcanic activity. The results typically support existing theories and previous external work, but reveal a strong dependence on datasets, time periods, and seasonal stratification. In some cases, results are counter to what is expected from existing scientific theories. During periods of enhanced vertical propagation of planetary waves (i.e. El Nino), the stratospheric polar vortex is slowed because of wave breaking in the stratosphere. This allows for subsequent subtropical cooling and polar warming at these levels, as well as facilitates the occurrence of SSW events. This is one way that a direct forcing by the troposphere may be felt by the stratosphere.

In the case of ENSO, supportive evidence is found from EP-Flux analyses that enhanced upward wave propagation from the troposphere, associated with constructive tropospheric interference of the El Nino PNA pattern and the climatological stationary waves, leads to a downward propagation of negative wind anomalies from the stratosphere at mid- latitudes. This deceleration of the stratospheric polar vortex, resulting from increased upward wave propagation, leads to expected equatorial (polar) stratospheric cooling (warming) in addition to an enhancement of tropospheric westerly jets. The meridional circulation induced by wave breaking is evident in stream function analyses of the NH during its cool season. Using the PV inversion technique, the study

revealed that a significant response in the tropospheric zonal mean winds at midlatitudes is forced by anomalous stratospheric potential vorticity within the ERA reanalyses data.

For the evolution of the QBO, the Holton-tan effect is evident in the zonal mean wind and EP-Fluxes analyses, though results from the stream function analyses and PV inversions do not clearly indicate a stratospheric influences on the troposphere. The QBO signal is the likely elusive using this linear approach because of the known influence of the seasonal cycle on the QBO, and its non-linear dynamics. We do not necessarily suggest that the results we have gathered are unsubstantiated; rather it suggests complexities within the system which are not easily addressed in a linear statistical framework.

Indication of the tropospheric response to stratospheric variability is evident in association with solar and volcanic forcing. When the temperature gradient within the stratosphere is altered via a change in incoming radiation, or aerosol loading, the vertical wind shear responds to maintain thermal wind balance. This has a direct impact on the ability of tropospheric planetary waves to enter these regions and also has a significant impact in the troposphere via downward control and induced meridional circulations.

In the case of volcanic activity, the analysis for the post-satellite time period incorporating extensive satellite data is less consistent with existing theories than the analysis for the extended time period that was witness to higher volcanic activity. When focused on the extended time period, enhanced volcanic aerosols are found to lead to strong stratospheric warming with an enhanced temperature gradient in the lower stratosphere and an enhanced stratospheric polar vortex in agreement with general scientific understanding. The enhanced vertical wind shear subsequently reduces

planetary wave propagation into that region, not seen in the post-satellite time period. This bolsters the argument that, to obtain robust signals from observational data, the data record must be reliable over an extended period of time. That length of time is closely associated with the innate frequency of the relevant forcing mechanism.

Though it is not evident from the results of the multivariate linear regression, the general circulation model experiments reveal that ozone heating of subtropical lower stratosphere and concomitent cooling of the troposphere below, as a result of UV blocking, leads to a strengthening and poleward shift of the stratospheric polar vortex. This sets up a positive feedback mechanism in which subsequent reduced wave propagation, caused by increased vertical wind shear, acts to further accelerate the zonal mean winds at high latitudes. This indirect mechanism is most evident in the model simulations, while little evidence of the meridonal deflection of tropospheric planetary waves is found in the observational analyses.

Evidence is found of a direct impact of the stratosphere on the troposphere through adjustments to geostrophic and hydrostatic balance after stratospheric redistributions of mass and potential vorticity. In particular, anomalous potential vorticity in the stratosphere associated with an increase in solar flux appears to induce an anomalous tropospheric circulation similar to that of the NAO. However, we find little evidence of the indirect mechanism seen in Kodera and Kuroda (2002) where the stratospheric polar vortex modulates tropospheric wave propagation allowing the radiatively driven state to persist longer during winter. It is possible that the signal may be lost in the current analysis by averaging over all winter months. The temporal variation of this mechanism complicates the extraction of this signal. Planetary waves

are unable to propagate into the strong jet and are instead meridionally deflected away from the center of circulation (Kodera and Kuroda 2002).

By comparison of the multivariate regression results with those of the general circulation model, it may be inferred that what actually happens in the stratosphere-troposphere climate system is likely more consistent with existing theory than what can be currently inferred from existing atmospheric reanalyses datasets. The dynamical relationships in the real atmosphere include those prescribed in the circulation models, but are complicated by nonlinearities and sampling issues such that conclusive confirmation of existing theories is not tractable with this form of analysis. Though no one analysis clearly offers conclusive evidence of the mechanisms at work, consistent evidence found among multiple diagnostic tools supports the existing scientific theories of the atmosphere's dynamic response to low frequency forcing.

REFERENCES

Andrews, D., J. Holton, and C. Levoy, Middle Atmosphere Dynamics, Academic Press, 1987.

Baldwin, M., T. Dunkerton, The Solar Cycle and Stratosphere- Troposphere Dynamical Coupling, J. Atmos. & Solar-Terr. Phys., 67, 71-82, 2004.

Baldwin, M., H. Edmon, J. Holton. A Diagnostic Study of Eddy-Mean Flow Interactions During FGGE SOP-1. J. Atmos. Sci., 42, 1838-1845, 1985.

Baldwin, M., L. Gray, T. Dunkerton, *et al*., The Quasi-Biennial Oscillation, Reviews of Geophysics, 32, 179-229, 2001.

Black, R.X., and B.A. McDaniel, Diagnostic Case Studies of the Northern Annular Mode J. Climate, 17, 3990-4004, 2004.

Boville, B. A., Wave-mean flow interactions in a general circulation model of the troposphere and stratosphere, J. Atmos. Sci., 43, 1711-1714, 1986

Chang, P., S. Zebiak, El Nino and the Southern Oscillation: Theory, Encyclopedia of Atmospheric Sciences Holton, J., Pyle, J., Curry, J, Academic Press, 719-723 2003.

Cordero, E., and T. Nathan, The Response of the QBO to Zonal-Mean Ozone Perturbations Consistent with the 11-year Solar Cycle, Solar Radiation and Climate Experiment (SORCE) Meeting, 2004.

Coughlin, K., and K. K. Tung, Eleven-year solar cycle signal throughout the lower atmosphere. J. Geophys. Res., 109, 2004.

Gleisner, H., Thejll, P., Patterns of Tropospheric Response to Solar Variability, Geophys. Res. Lets., Amer. Geophys. Union, 41-44, 2003.

Grotjahn, R., General Circulation: Mean Characteristics. Encyclopedia of Atmospheric Sciences, J. Holton, J. A. Curry, and J. Pyle, Eds., Academic Press, London, 841-854, 2003.

Haigh, J. D., Solar Terrestrial Interactions, Encyclopedia of Atmospheric Sciences, Holton, J. Pyle, J., Curry, J., 2072-2078, 2003.

Haigh, J. D., The effects of Solar Variability on the Earth's Climate, Phil. Trans.: Math., Phys. and Eng. Sci., Royal Society of London, 361, 95 – 111, 2003.

Haigh, J. D. et al., Solar Variability and Climate: Selected Results from the SOLICE Project, Stratospheric Processes and their Role in Climate, World Climate Research Programme, 2004.

Haigh J., M. Blackburn, and R. Day, The response of tropospheric circulation to perturbations in lower stratospheric temperature, Journal of Climate, 18, 3672 - 3691, 2005.

Haigh, J., Climate variability and the influence of the sun, Science, 294, 2109 – 2111, 2001.

Hameed, S., and J. Lee, A mechanism for sun-climate connection, Geophys. Res. Lett., 32, L23817, 2005.

Haynes, P., Stratospheric dynamics. Ann. Rev. Fluid Mech., 37:263-293, 2005

Holton, J., Dynamic Meteorology: Waves. Encyclopedia of Atmospheric Sciences, J. Holton, J. A. Curry, and J. Pyle, Eds., Academic Press, London, 841-854, 2003.

Holton, J., P. Haynes, M. McIntyre, A. Douglass, R. Rood, and L. Pfister, Stratosphere-troposphere exchange, Rev. Geophys., 33, 403-439, 1995.

Hurrell, J.W., Climate Variability: North Atlantic and Arctic Oscillation. Encyclopedia of Atmospheric Sciences, Holton, J., Pyle, J., Curry, J., 439-445, 2003.

Kalnay, E., et al., The NCEP/NCAR 40-year reanalysis project. Bull. Amer.Meteor. Soc., 77, 437-471, 1996.

Kodera, K., Y. Kuroda, Dynamical Response to the Solar Cycle, J. Geophys. Res., 107, ACL5, 2002.

Kodera, K., Y. Kuroda, A Possible Mechanism of Solar Modulation of the Spatial Structure of the North Atlantic Oscillation, J. Geophys. Res., 110, 2005.

Kodera, K., Solar influence on the spatial structure of the NAO During the. winter 1900–1999, Geophys. Res. Lett., 30(4), 1175, 2003.

Kuroda, Y. and K. Kodera, Solar cycle modulation of the Southern Annular Mode, Geophys. Res. Lett., 32, L13802, 2005.

Labitzke, K., The Global Signal of the 11-year Sunspot Cycle in the Stratosphere: Differences Between Solar Maxima and Minima, Meteologische Zeitschrift, 10, 83-90, 2000.

Lee, H. and A. Smith, Simulation of the combined effects of solar cycle, quasi- biennial oscillation and volcanic forcing on stratospheric ozone changes in recent decades, J. Geophys. Res., 108, 2003.

Lewis, R. P. W., Ed., Meteorological Glossary. 6th ed. Her Majesty's Stationer's Office, 335, 1991.

Lorenz, D., and D. Hartmann, Eddy-Zonal flow feedback in the Northern Hemisphere Winter. J. Climate, 16(8), 1212-1227. 2003.

Matsuno, T., A dynamical model of the stratospheric sudden warming. Journal of the Atmospheric Sciences, 28(8), 1479-1494, 1971.

McCaa, J., et al., Users Guide to the NCAP Community Atmosphere Model (CAM 3.0), Climate and Global Dynamics Division, National Center for Atmospheric Research, Boulder, Colorado, June 2004.

McCormack, J., Decadal Variability in the Sun and Climate, Solar Radiation and Climate Experiment (SORCE) Meeting, 2004.

Nicholls, N., El Nino and the Southern Oscillation: Observation, Encyclopedia of Atmospheric Sciences Holton, J., Pyle, J., Curry, J., Academic Press, 713-718, 2003.

Palmer, T. N., Properties of Eliassen-Palm Flux for Planetary Scale Motions, J. Atmos. Sci., 39, 992-997, 1983.

Plumb, R. and K. Semeniuk, Downward migration of extratropical zonal wind anomalies. J. Geophys. Res., 108 (D7), 4223, 2003.

Reid, G., Solar variability and its implications for the human environment, J. Atmos. & Solar-Terr. Phys., 61, 3-14, 1999.

Robock, Introduction: Mount Pinatubo as a Test of Climate Feedback Mechanisms, Volcanism & the Earth's Atmosphere., American Geophysical Union, Geophysical Monograph 139, 2003.

Robock, A., Volcanoes: Role in climate. Encyclopedia of Atmospheric Sciences, J. Holton, J. A. Curry, and J. Pyle, Eds., Academic Press, London, 2494-2500, 2003.

Rottman, G., Solar Ultraviolet Irradiance and its Temporal Variation, J. Atmos. & Solar-Terr. Phys., 61, 37-44, 1999.

Rozanov, E., et al., Atmospheric response to the observed increase of solar UV radiation from solar minimum to solar maximum simulated by the UIUC climate-chemistry model, J. Geophys., 109, 2004.

Sato, M., Stratospheric Aerosol Optical Depths, 1850-1990, J. Geophys. Res., 98, 22987-22993, 1993.

Shepherd, T.G., 2002: Issues in stratosphere-troposphere coupling. J. Meteorol. Soc. Jpn., 80, 769-792.

Smith, A. K. Middle Atmosphere: Planetary Waves, Encyclopedia of Atmospheric Sciences Holton, J., Pyle, J., Curry, J, Academic Press, 1314-1321, 2003.

Song, Y. and W. Robinson, Dynamical Mechanisms for Stratospheric. Influences on the Troposphere. J. Atmos. Sci, 61, 1711–1725, 2004.

Tinsley, B., W. Hanson Center for Space Science, University of Texas at Dallas, 2004

Taguchi, M., and D. Hartman, Interference of extratropical surface climate anomalies induced by El Nino and stratospheric sudden warmings. Geophysical Research Letters 32(4): L04709, 2005.

Thompson, D., J. Furtado, and T. Shepherd, The "Direct Effect" of stratospheric variability on the troposphere. J. Atmos. Sci., 2005

Wallace, J., P. Hobbs, Atmospheric Science: An Introductory Survey, Academic Press, London, 322-327, 1977.

Wallace, J., General Circulation: Overview. Encyclopedia of Atmospheric Sciences, J. Holton, J. A. Curry, and J. Pyle, Eds., Academic Press, London, 821-829, 2003.

Zhou, S., A. J. Miller, Sensitivity of Stratospheric Zonal Wind to Solar Variations, Solar Radiation and Climate Experiment (SORCE) Meeting, 2004.